Multi-layer Unmanned Aerial Vehicle Networks: Modeling and Performance Analysis

Dongsun Kim, *Student Member, IEEE*, Jemin Lee, *Member, IEEE*, and Tony Q. S. Quek, *Fellow, IEEE*

***Abstract*— In this paper, we establish a foundation for the multi-layer aerial networks (MANs), which are modeled as K layer aerial networks (ANs), where each layer has unmanned aerial vehicles (UAVs) with different densities, floating altitudes, and transmission power. To make the framework applicable for various scenarios in MAN, we consider the transmitter- and the receiver-oriented node association rules as well as the air-to-ground and air-to-air channel models, which form line of sight links with a location-dependent probability. We then newly analyze the association probability, the main link distance distribution, successful transmission probability (STP), and area spectral efficiency (ASE) of MAN. The upper bounds of the optimal densities that maximize STP and ASE are also provided. Finally, in the numerical results, we show the optimal UAV densities of each AN that maximize the ASE and the STP decrease with the altitude of the network. We also show that when the total UAV density is fixed for two layer AN, the use of single layer in higher(lower) altitude only for all UAVs can achieve better performance for low(high) total density case. Otherwise, distributing UAVs in two layers, i.e., MAN, achieves better performance.**

***Index Terms*— Aerial networks, multiple network layer, unmanned aerial vehicles, stochastic geometry, line of sight (LoS) probability.**

I. Introduction

RECENT development of the UAV technologies enables the UAV to play various roles in the wireless networks. The UAVs are expected to work as temporal base stations (BSs) in case of the disaster and the data demanding events [2], and the data acquisition for the crowd surveillance can also be done by UAVs [3]. Furthermore, the UAVs can act as relays for unreliable direct link case [4]. As such demands on the UAV communications and the number of UAVs increase, the research for the reliable AN must be preceded.

The UAV based wireless communication has been studied in [5]–[10] after modeling the wireless channel and the mobility, which are different from those of the terrestrial networks. In [5], the probability that a link forms LoS, i.e., the LoS probability, is modeled, which is determined by the angle from the ground, and also proposed the optimal UAV deployment that maximizes the coverage area. The path loss and the channel gain of the link between a UAV and a ground node are studied in [6]. In [7], the LoS probability is provided for the link between UAVs, which have different altitudes. Considering LoS channel, device-to-device communications, secrecy capacity UAV-aided communication systems, and UAV to ground communication in presence of interferer are studied in [8], [9], and [10], respectively. However, the studies mentioned above have considered only the small number of UAVs, which show the performance of the limited UAV communication scenarios.

Recently, the researches on the ANs, which is the wireless networks consisting of UAVs, have been presented in [11]–[25]. For those works, the stochastic geometry has been used, which is a widely-used tool for randomly distributed nodes [26]. The 2-D Poisson point process (PPP)-based ANs model is presented and studied in [11]–[19], the 2-D binomial point process (BPP)-based model is studied in [20], [23], where random altitude of UAVs is considered [17]–[19]. Furthermore, the research on the coexistence of an AN with the terrestrial network is presented in [14]–[22]. In these works, the nodes in the terrestrial network are modeled by a PPP. Especially, in [21] and [22], the distribution of ground users (receivers) are modeled by a clustering point process (for disaster area or temporal data demanding events like a concert) [21] and a PPP [22]. In addition, the throughput maximization of the AN is studied in [27]–[29] by jointly optimizing the trajectory and resource allocation in [27], while the game theory is used to allocate the bandwidth and to choose UAV BS pairs in [29]. In [28], the number of users that successfully served by a UAV is maximized by optimizing the position of a UAV. However, most of these works did not consider the multiple layer structure of AN, of each layer has different types of UAVs.

Since the applications of UAVs increase, it becomes more important to utilize the limited aerial space efficiently.

Manuscript received April 1, 2019; revised August 16, 2019; accepted September 11, 2019. Date of publication October 4, 2019; date of current version January 8, 2020. This work was supported in part by the Daegu Gyeongbuk Institute of Science and Technology (DGIST) Research and Development Program of the Ministry of Science and ICT under Grant 17-ST-02, in part by the National Research Foundation of Korea (NRF) grant funded by the Korea government (MSIT) under Grant NRF-2018R1A5A1060031, and in part by the Institute for Information and communications Technology Promotion (IITP) grant funded by the Korea government (MSIT) under Grant 2018-0-01410, Development of Radio Transmission Technologies for High Capacity and Low Cost in Ultra Dense Networks. This article was presented in part at the IEEE Global Communications Conference, UAE, December 2018 [1]. The associate editor coordinating the review of this article and approving it for publication was C.-K. Wen. *(Corresponding author: Jemin Lee.)*

D. Kim and J. Lee are with the Department of Information and Communication Engineering, Daegu Gyeongbuk Institute of Science and Technology, Daegu 42988, South Korea (e-mail: yidaever@dgist.ac.kr; jmnlee@dgist.ac.kr).

T. Q. S. Quek is with the Information Systems Technology and Design Pillar, Singapore University of Technology and Design, Singapore 487372 (e-mail: tonyquek@sutd.edu.sg).

Color versions of one or more of the figures in this article are available online at http://ieeexplore.ieee.org.

Digital Object Identifier 10.1109/TWC.2019.2944378

Furthermore, the altitude, where the UAVs float, will be limited due to the UAV flight regulation [30] or the hardware constraint [31]. Therefore, it will be impossible to allocate a unified range of altitude for all UAVs in an AN, which makes the *separation of the AN into multi-layered ANs inevitable*. Motivated from this, we study the MAN, which consists of K-layers of ANs. Note that layered structure of AN is also presented in [24], [25], and [22]. In [24] and [25], the UAVs are used as relays [24] or downlink base stations to improve the downlink spectral efficiency [25]. However, the analysis result on the performance has not been provided, especially in terms of the successful transmission probability (STP) or the area spectral efficiency (ASE) of the multiple layer structure AN. In [22], the spectral efficiency of multiple layer structure AN was analyzed by focusing on the communications of ground base stations, assisted by UAVs. However, in [22], only the performance of the single layer AN case is provided in the simulation results and the communication between UAVs are not considered, which fails to fully explore the efficient design of the multiple layer AN.

Therefore, in this paper, we provide a general framework of the MAN, which consists of K-layers of ANs that have UAVs with different altitudes, spatial densities, and transmission power. We then analyze the STP and the ASE of the MAN and figure out the effects of the parameters on the performance. Furthermore, we analyze the effects of the altitude and the density of UAVs on the performance of the MAN to provide guidelines for the efficient design of the MAN. The contribution of this work can be summarized as follows.

- Differently to prior works on aerial networks and terrestrial heterogeneous networks, we model the MAN by considering both the node association rules and channel model, suitable for various scenarios of the MAN. Specifically, according to the association subject, we consider two types: the *transmitter-oriented* association (e.g., when a transmitting UAV selects the best receiving BS) and the *receiver-oriented* association (e.g., when a receiving UAV selects the best transmitting BS). Furthermore, we consider both air-to-air (A2A) and air-to-ground (A2G) channels, which form LoS links with a certain probability, influenced by not only the link distance but also the UAV altitude.
- We newly analyze the Laplace transform of the interference considering LoS and NLoS channel, which is required to analyze the STP and the ASE. Especially, the Laplace transform of the interference from the same layer UAVs is provided in a closed form. Note that the multiple layer structure has been considered for terrestrial networks, called as the heterogeneous networks [32]–[34], and the Laplace transform of the interference has also been analyzed. However, as the node association rules and the channel model, suitable for MAN, are used in this work, the analysis has been newly performed.
- We then analyze the STP and the ASE of the MAN using stochastic geometry. We also provide the upper bound of the optimal transmitting UAV densities for each layer, which maximize the STP and the ASE. This is the first work, optimizing the node density of AN, to the best knowledge of the authors.
- We finally provide insights on the efficient design of MAN via numerical results. Specifically, we provide the optimal altitude and the densities of UAV in each layer in terms of the STP and the ASE, and also show when the multiple layer structure of AN can achieve better performance than the single layer AN.

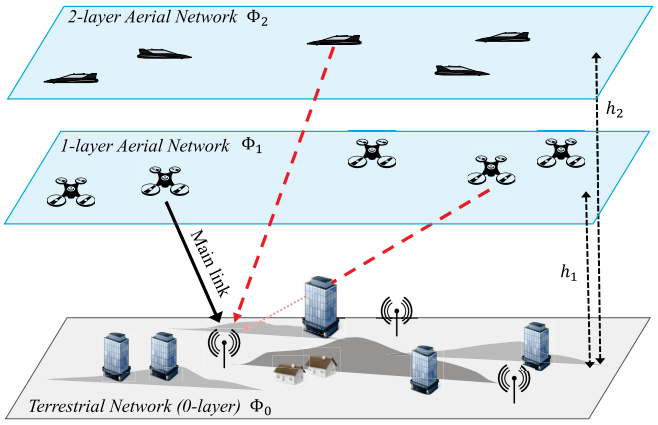

Fig. 1. An example of two layer MAN with ground receivers (i.e., 0-layer). The black lines represent the main link and red dashed lines represent interference links.

II. System Model

In this section, we present the system model of a MAN including the network description and the channel model. Furthermore, we describe the node association rules and present the probability distribution function (PDF) of the main link distance.

A. Multi-layer Aerial Network Structure

We consider a MAN, which consists of K layers of AN at different altitudes as shown in Fig. 1. We denote $\mathcal{K}$ as the set of layers constituting the MAN, i.e., $\mathcal{K} = \{0, 1, \cdots, K\}$, where layer 0 is specially used for the ground layer. The nodes in the ground layer can act as the ground users or the base stations, which can generate interference or provide service, that is the coexistence of the AN with the ground layer as studied in [16]. Note that without modifying the analysis, the base station with non-zero antenna height [35] can be considered which is the same with the AN layer with the low altitude. Furthermore, the coexistence with the heterogeneous networks also can be considered in the MAN by adding the ground layers. We assume UAVs in ANs are distributed according to 2D-PPPs with a fixed floating altitude such as in [14], [36] as well as the ground user and the base station layers [26]. Even though our analysis focused on the MAN with the fixed AN altitude, our analysis can be expanded for the case when the altitude follows random variables, that is studied in [19] where the UAV uniformly folate between the maximum and the minimum altitude. Specifically, in the k-layer, the node locations follow a homogeneous 2D-PPP Φ_k with density λ_k,

TABLE I
NOTATIONS USED THROUGHOUT THE PAPER

Notation	Definition
$\mathcal{K}$	Set of layers constituting the MAN
K	Number of ANs distributed in 2D-PPP
h_k	Altitude of the k-layer nodes
P_k	Transmission power of the k-lyaer nodes
$\lambda_{k,\mathrm{Rx(Tx)}}$	Density of the receivers(transmitters) in the k-layer
$\Phi_{k,\mathrm{Rx(Tx)}}$	Distribution of the receiver(transmitter) in the k-layer
$c \in \{\mathrm{L},\mathrm{N}\}$	Indicator whether the channel is LoS or NLoS
$\alpha_{ij}^{(c)}$	Path loss exponent of channel c between i and j layer
$G_{ij}^{(c)}$	Channel gain of channel c between i and j layer
$m_{ij}^{(c)}$	Shape parameter of Nakagami-m fading for ghannel gain $G_{ij}^{(c)}$
$\rho_{ij}^{(c)}(x)$	Probability that link between the i-layer receiver and the j-layer transmitter is under channel environment c when the link distance is x
$\tau = oa$	Communication node association rule defined by o and a
$o \in \{\mathrm{r},\mathrm{t}\}$	Node association rule that indicates whether the communication is the receiver-oriented or the transmission oriented association
$a \in \{\mathrm{n},\mathrm{s}\}$	Node association rule that indicates whether the node with the nearest distance or the strongest power is selected
$\mathcal{A}_{ij,\tau}^{(c)}$	Probability that the main link is established between the i and j-layer nodes under channel c using association rule τ
$Y_{ij,\tau}^{(c)}$	Random variable that represents the main link distance given association $\mathcal{A}_{ij,\tau}^{(c)}$
$I_{ij}^{(c)}$	Interference to the i-layer receiver from j-layer transmitters in the channel c
$\mathcal{I}_i$	Sum of the interference and noise to the i-layer receiver
χ	Distance that indicates the area where the interferer cannot exist
$\varepsilon_{ij,\tau}^{(c)}(y)$	Event when the main link is established between i and j-layer with distance y using the node association rule τ
$\mathcal{L}_{I\|\varepsilon_{ij,\tau}^{(c)}(y)}$	Laplace transform of the I in the event of $\varepsilon_{ij,\tau}^{(c)}(y)$
$p_{ij,\tau}^{(c)}(y)$	STP in the event of $\varepsilon_{ij,\tau}^{(c)}(y)$
$\mathcal{P}_{k,\tau}$	STP of the k-layer in the MAN
$\mathcal{S}_{k,\tau}$	ASE of the k-layer in the MAN [bps/Hz/m^2]
$\lambda_{j,\mathrm{Tx}}^{b,\mathcal{P}_{k,\tau}(\mathcal{S}_{k,\tau})}$	Upper bound of the optimal transmitter density in the j-layer that maximizes the STP(ASE) of k-layer

and they are at the fixed altitude h_k and transmit with the power P_k. In the k-layer, nodes act as either a receiver or a transmitter, where the set of the receivers and the transmitters are denoted by $\Phi_{k,\mathrm{Rx}}$ and $\Phi_{k,\mathrm{Tx}}$. Similarly, the densities of the receivers and the transmitters in the k-layer are given by $\lambda_{k,\mathrm{Rx}}$ and $\lambda_{k,\mathrm{Tx}}$. Here, $\Phi_k = \Phi_{k,\mathrm{Rx}} + \Phi_{k,\mathrm{Tx}}$ and $\lambda_k = \lambda_{k,\mathrm{Rx}} + \lambda_{k,\mathrm{Tx}}$ and the altitudes of layers are $h_k \geq 0$ for $k \in \mathcal{K}$. In addition, the altitude between the i-layer and the j-layer is denoted by $h_{ij} = |h_i - h_j|$.

B. Channel Model

We consider both LoS and non-line of sight (NLoS) links, which have different path loss exponents and channel fading models. For the link between i- and j- layer nodes, the path loss exponents for LoS and NLoS links are respectively denoted by $\alpha_{ij}^{(\mathrm{L})}$ and $\alpha_{ij}^{(\mathrm{N})}$, and generally, $2 \leq \alpha_{ij}^{(\mathrm{L})} \leq \alpha_{ij}^{(\mathrm{N})}$. The channel experiences the Nakagami-m fading, so the channel gain for LoS and the NLoS links are respectively presented by $G_{ij}^{(\mathrm{L})} \sim \Gamma(m_{ij}^{(\mathrm{L})}, \frac{1}{m_{ij}^{(\mathrm{L})}})$ and $G_{ij}^{(\mathrm{N})} \sim \Gamma(m_{ij}^{(\mathrm{N})}, \frac{1}{m_{ij}^{(\mathrm{N})}})$. Here, $m_{ij}^{(\mathrm{c})} \geq 1$, $\forall c = \{\mathrm{L},\mathrm{N}\}$, and $m_{ij}^{(\mathrm{c})} = 1$ means Rayleigh fading, i.e., $G_{ij}^{(\mathrm{N})} \sim \exp(1)$. Note that the indexes i, j are used in $\alpha_{ij}^{(\mathrm{c})}$ and $m_{ij}^{(\mathrm{c})}$ since the channel models including $\alpha_{ij}^{(\mathrm{c})}$ and $m_{ij}^{(\mathrm{c})}$ can also be determined differently according to the altitudes of the layers as studied in [37].

In the terrestrial network, where the transmitter and the receiver are on the ground, the link is generally modeled as NLoS. However, in the MAN, we have the communication between a UAV and a ground node as well as the communication between UAVs. For those communications, whether the link is LoS or NLoS is determined by the existence of obstacles (e.g., buildings) between the transmitter and the receiver [5], [7] by following the ITU model [38]. In this paper, we define the probability of forming LoS link as the LoS probability $\rho_{ij}^{(\mathrm{L})}(x)$ and the probability of forming NLoS link as the NLoS probability $\rho_{ij}^{(\mathrm{N})}(x) = 1 - \rho_{ij}^{(\mathrm{L})}(x)$, where a receiver and a transmitter are in the i-layer and the j-layer, respectively, and the link distance is x. From [5], the LoS probability is given by

$$\rho_{ij}^{(\mathrm{L})}(x) = \prod_{n=0}^{M} \left[1 - \exp\left(- \frac{\left[\max(h_i, h_j) - \frac{(n+1/2)h_{ij}}{M+1} \right]^2}{2\xi^2} \right) \right] \quad (1)$$

where $M = \mathrm{floor}\left(\sqrt{(x^2 - h_{ij}^2)\mu\nu} - 1 \right)$. Here, μ, ν, and ξ are the parameters related to the environments [38], where μ is the ratio of area covered by buildings to total area, ν is the mean number of buildings per unit area, and ξ is the average altitude of buildings. Specifically, for the A2G channel (i.e., $i = 0$ or $j = 0$, and $i \neq j$) and the A2A channel (i.e., $i \neq 0$ and $j \neq 0$), $\rho_{ij}^{(\mathrm{L})}(x)$ is given by

$$\rho_{ij}^{(\mathrm{L})}(x) \approx$$

$$\begin{cases} \dfrac{1}{1 + \iota \exp\left(-\kappa \left[\sin^{-1}\left(\dfrac{h_{ij}}{x} \right) - \iota \right] \right)} & i \text{ or } j = 0,\ i \neq j \quad (2) \\ \left(1 - \exp\left\{ -\dfrac{h_i^2}{2\xi^2} \right\} \right)^{x\sqrt{\nu\mu}} & i, j \neq 0,\ i = j \quad (3) \\ \left(1 - \dfrac{\sqrt{2\pi}\xi}{h_{ij}} \left| Q\left(\dfrac{h_i}{\xi} \right) - Q\left(\dfrac{h_j}{\xi} \right) \right| \right)^{\sqrt{(x^2 - h_{ij}^2)\nu\mu}} & i, j \neq 0,\ i \neq j \quad (4) \end{cases}$$

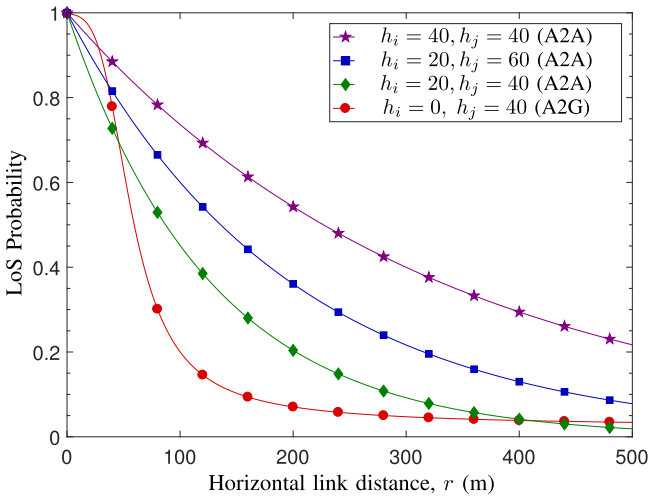

Fig. 2. LoS channel probability according to the horizontal distance r with different receiver and transmitter altitudes h_i and h_j.

where ι and κ are related to ν, μ, and ξ [5], and $Q(x) = \int_x^\infty \frac{1}{\sqrt{2\pi}} \exp\left(-\frac{x^2}{2}\right) dx$. Here, (2) is obtained using sigmoid function based approximation [5] , (3) and (4) are obtained using exponential function based approximation [39].[1] The LoS channel between ground nodes is given by $\rho_{ij}^{(\mathrm{L})}(x) = 0$.

From (2)-(4), we can see that the LoS probability is affected by both the horizontal distance and the altitude difference between the transmitter and the receiver, and this is shown in Fig. 2. Figure 2 shows the LoS probability as a function of the horizontal distance $r = \sqrt{x^2 - h_{ij}^2}$ for A2A and A2G channels in the dense urban environment.[2] We observe that the LoS probability decreases with r since the larger distance generally has more blockages, which causes the NLoS environment. On the contrary, the LoS probability increases not only with the altitude difference between the transmitter and receiver, h_{ij}, but also with altitudes of the transmitter and the receiver, h_i and h_j.

Based on the LoS probability, we define $\Phi_{ij,\mathrm{Tx}}^{(\mathrm{L})}$ and $\Phi_{ij,\mathrm{Tx}}^{(\mathrm{N})}$ as the set of transmitters in the j-layer which have LoS and NLoS channels to a receiver in the i-layer. Similarly, we define $\Phi_{ij,\mathrm{Rx}}^{(\mathrm{L})}$ and $\Phi_{ij,\mathrm{Rx}}^{(\mathrm{N})}$ as the set of receivers in the i-layer, which have LoS and NLoS channels to a transmitter in the j-layer, respectively. Let $\Phi_{ij,\mathrm{Tx}}^{(c)}(x)$ be the set of points, which are located with the distance x from the typical i-layer receiver, in $\Phi_{ij,\mathrm{Tx}}$. Then, by the mapping theorem [26], $\Phi_{ij,\mathrm{Tx}}^{(c)}(x)$ becomes an inhomogeneous PPP with the density function $2\pi x \lambda_{i,\mathrm{Rx}} \rho_{ij}^{(c)}(x)$ for all $c \in \{\mathrm{L}, \mathrm{N}\}$, which will be used in the analysis of the main link distance distribution and the Laplace transform of the interference.

C. Communication Node Association Rules

The node association rule is used to determine which BS a node needs to connect for communications in the terrestrial networks. For instance, a node can select the nearest BS from the location information (called as the *nearest node association*) or the BS with the strongest strength of the received pilot signals from BSs (called as the *strongest node association*) [35].

Similarly, in the MAN, when a UAV wants to receive some data from a BS, the UAV (i.e., the receiver) can select the best BS (i.e., the transmitter) among BSs, which we call it as the *receiver-oriented* association. On the other hand, when a UAV wants to transmit some data (e.g., surveillance data) to a BS, the UAV can select the best BS as a transmitter, which we call it as the *transmitter-oriented* association.[3] In order to embrace those various association scenarios, we introduce the association parameter τ as

$$\tau = o \cdot a \tag{5}$$

where o represents the association subjective, i.e., $o = \mathrm{t}$ for the transmitter-oriented and $o = \mathrm{r}$ for the receiver-oriented association. In (5), a represents the association criterion, i.e., $a = \mathrm{s}$ for the strongest node association and $a = \mathrm{n}$ for the nearest node association. For example, $\tau = \mathrm{rs}$ means the receiver associates to the transmitter with the strongest received power.

Based on $\tau = oa$, the coordinate of the associated node for a node at $\mathbf{x}$ is defined as

$$\mathbf{x}_\tau = \begin{cases} \underset{\mathbf{x} \in \Phi_{k,o}, k \in \mathcal{K}}{\arg\max}\ B_k |\mathbf{x} - \hat{\mathbf{x}}|^{-1} & \text{for } a = \mathrm{n}, \\ \underset{\mathbf{x} \in \Phi_{k,o}, k \in \mathcal{K}}{\arg\max}\ B_k |\mathbf{x} - \hat{\mathbf{x}}|^{-\alpha_{\mathbf{x}}} & \text{for } a = \mathrm{s}, \end{cases} \tag{6}$$

where B_k is the association bias of k-layer, $\alpha_{\mathbf{x}}$ is the path loss exponent of the link between a transmitter and a receiver where the node $\mathbf{x}$ is involved. In (6), $\Phi_{k,o}$ is set of candidates, considered in the association. That means, when $o = \mathrm{r}$, since the receiver selects the best one among transmitters, $\Phi_{k,\mathrm{r}} = \Phi_{k,\mathrm{Tx}}$. Similarly, when $o = \mathrm{t}$, since the best one among receivers is selected, $\Phi_{k,\mathrm{t}} = \Phi_{k,\mathrm{Rx}}$.

D. Main Link Distance Distribution Analysis

In conventional terrestrial networks, the PDF of the main link distance is influenced by the transmission power, the path loss exponent, and the link distance. However, in an AN, we also need to consider the LoS/NLoS probabilities associated with the link. For the association $\tau = oa$, the PDF of the main link distance is presented in the following lemma. Note that in the following Lemma, we use $f_X(x)$, $F_X(x)$, and $\bar{F}_X(x)$ to represent the PDF, cumulative distribution function (CDF), and complementary cumulative distribution function (CCDF) of a random variable X, respectively.

Lemma 1: Using the node association rule τ, when main link is established between a receiver in the i-layer and a transmitter in the j-layer under the channel environment c,

[1]Similar result with the same approach is provided in the [7], however, we follow the [39] to provide well-matched approximation with our model.

[2]The parameters used in this figure are $\mu = 0.5$, $\nu = 3 \times 10^{-4}$ (buildings/m^2), $\xi = 20$ (m), $a = 12.0810$, and $b = 0.1139$ [5].

[3]Note that depending on the association subjective (i.e., whether the transmitter or the receiver selects the best node), the main link distance as well as the average number of communicating links in the network, used to define the ASE need to be determined differently, which will be shown in Lemma 1 and (31) of Theorem 1.

the PDF of main link distance $Y_{ij,\tau}^{(c)}$ is given by

$$f_{Y_{ij,\tau}^{(c)}}(y) = \frac{f_{V_{ij,o}^{(c)}}(y)}{\mathcal{A}_{ij,\tau}^{(c)}} \prod_{\substack{k\in\mathcal{K},c_{\rm o}\in\{\rm L,N\},\\(k,c_{\rm o})\neq(j,c)}} \bar{F}_{V_{ik,o}^{(c_{\rm o})}}\left(R_{ij,k,a}^{(c,c_{\rm o})}(y)\right), \quad (7)$$

where $R_{ij,k,a}^{(c,c_{\rm o})}(y)$ is the minimum distance between the i-layer receiver and a transmitter in k-layer under channel c, given by

$$R_{ij,k,a}^{(c,c_{\rm o})}(y) = \begin{cases} yB_k/B_j & \text{for } a = \text{n}, \\ \left(y^{\alpha_{ij}^{(c)}} B_k/B_j\right)^{1/\alpha_{ik}^{(c_{\rm o})}} & \text{for } a = \text{s}. \end{cases} \quad (8)$$

and $\mathcal{A}_{ij,\tau}^{(c)}$ is the association probability given by

$$\mathcal{A}_{ij,\tau}^{(c)} = \int_{x>0} f_{V_{ij,o}^{(c)}}(x) \prod_{\substack{k\in\mathcal{K},c_{\rm o}\in\{\rm L,N\},\\(k,c_{\rm o})\neq(j,c)}} \bar{F}_{V_{ik,o}^{(c_{\rm o})}}\left(R_{ij,k,a}^{(c,c_{\rm o})}(x)\right) dx. \quad (9)$$

Here, $V_{ik,o}^{(c_{\rm o})}$ is the distance to the nearest node among the nodes in the k-layer AN under the channel environment $c_{\rm o} \in \{\text{L,N}\}$ from a node in the i-layer, of which the CCDF and the PDF are given by

$$f_{V_{ik,o}^{(c_{\rm o})}}(v) = 2\pi\lambda_{k,o} v \rho_{ik}^{(c_{\rm o})}(v) \exp\left(-\int_{h_{ik}}^{v} 2\pi\lambda_{k,o} x \rho_{ik}^{(c_{\rm o})}(x) dx\right),$$
$$\bar{F}_{V_{ik,o}^{(c_{\rm o})}}(v) = \exp\left(-\int_{h_{ik}}^{\max(v,h_{ik})} 2\pi\lambda_{k,o} x \rho_{ik}^{(c_{\rm o})}(x) dx\right), \quad (10)$$

where $f_{V_{ik,o}^{(c_{\rm o})}}(v) = 0$ if $v \geq h_{ik}$.

Proof: From the LoS probability, the density function of $\Phi_{ij,\text{Tx}}^{(c)}(x)$ is given by $2\pi x\lambda_{k,o}\rho_{ik}^{(c_{\rm o})}(x)$. Therefore, the CDF of $V_{ik,o}^{(c_{\rm o})}$ is given by

$$F_{V_{ik,o}^{(c_{\rm o})}}(v) \overset{(a)}{=} 1 - \exp\left(-\int_{h_{ik}}^{\max(v,h_{ik})} 2\pi\lambda_{k,o} x \rho_{ik}^{(c_{\rm o})}(x) dx\right) \quad (11)$$

where (a) is from the void probability of PPP. From (11), we have (10).

In the nearest distance association case, the main link has the smallest distance, hence, the probability that main link is established as $\mathbf{x}_\tau \in \Phi_{ij,o}^{(c)}$ and the main link distance is smaller than y is given by

$$\begin{aligned}
&\mathbb{P}\left(V_{ij,o}^{(c)} \leq y,\ \mathbf{x}_\tau \in \Phi_{ij,o}^{(c)} \mid a = \text{n}\right) \\
&= \int_0^y f_{V_{ij,o}^{(c)}}(v) \mathbb{P}\left(\mathbf{x}_\tau \in \Phi_{ij,o}^{(c)} \,\middle|\, V_{ij,o}^{(c)} = v, a = \text{n}\right) dv \\
&\overset{(a)}{=} \int_0^y f_{V_{ij,o}^{(c)}}(v) \prod_{\substack{k\in\mathcal{K},c_{\rm o}\in\{\rm L,N\},\\(k,c_{\rm o})\neq(j,c)}} \mathbb{P}\left[\frac{B_j}{v} \geq \frac{B_k}{V_{ik,o}^{(c_{\rm o})}}\right] dv \\
&= \int_0^y f_{V_{ij,o}^{(c)}}(v) \prod_{\substack{k\in\mathcal{K},c_{\rm o}\in\{\rm L,N\},\\(k,c_{\rm o})\neq(j,c)}} \mathbb{P}\left[R_{ij,k,\text{n}}^{(c,c_{\rm o})}(y) \leq V_{ik,o}^{(c_{\rm o})}\right] dv, \quad (12)
\end{aligned}$$

where (a) is from (6). Here, for $y \to \infty$, the probability becomes $\mathbb{P}\left[\mathbf{x}_\tau \in \Phi_{ij,o}^{(c)} \mid a = \text{n}\right]$, which is association probability in (9). In the strongest power association case, the main link has the strongest signal power, hence, the probability that main link is established as $\mathbf{x}_\tau \in \Phi_{ij,o}^{(c)}$ and the main link distance is smaller than y is given by

$$\begin{aligned}
&\mathbb{P}\left(Y_{ij,\tau}^{(c)} \leq y,\ \mathbf{x}_\tau \in \Phi_{ij,o}^{(c)} \mid a = \text{s}\right) \\
&\overset{(a)}{=} \int_0^y f_{V_{ij,o}^{(c)}}(v) \prod_{\substack{k\in\mathcal{K},c_{\rm o}\in\{\rm L,N\},\\(k,c_{\rm o})\neq(j,c)}} \mathbb{P}\left[\frac{B_j}{v^{\alpha_{ij}^{(c)}}} \geq \frac{B_k}{\left(V_{ik,o}^{(c_{\rm o})}\right)^{\alpha_{ik}^{(c_{\rm o})}}}\right] dv \\
&= \int_0^y f_{V_{ij,o}^{(c)}}(v) \prod_{\substack{k\in\mathcal{K},c_{\rm o}\in\{\rm L,N\},\\(k,c_{\rm o})\neq(j,c)}} \mathbb{P}\left[R_{ij,k,\text{s}}^{(c,c_{\rm o})}(y) \leq V_{ik,o}^{(c_{\rm o})}\right] dv, \quad (13)
\end{aligned}$$

where (a) is from (6). Therefore, we derived the association probability (9) by $y \to \infty$.

Finally, the CDF of main link distance $Y_{ij,\tau}^{(c)}$ is given by

$$F_{Y_{ij,\tau}^{(c)}}(y) = \mathbb{P}\left(V_{ij,o}^{(c)} \leq y,\ \mathbf{x}_\tau \in \Phi_{ij,o}^{(c)}\right) / \mathcal{A}_{ij,\tau}^{(c)}, \quad (14)$$

which gives (7). ■

E. Performance Metric

In this subsection, we introduce the signal to interference plus noise ratio (SINR) and the STP. The interference to the i-layer receiver from the transmitters in the k-layer AN, which have LoS links ($c_{\rm o} = \text{L}$) and NLoS links ($c_{\rm o} = \text{N}$) to the receiver is given by

$$I_{ik}^{(c_{\rm o})} = \sum_{\mathbf{x}\in\Phi_{ik,\text{Tx}}^{(c_{\rm o})}/\mathbf{x}_\tau} P_k G_{ik}^{(c_{\rm o})} x^{-\alpha_{ik}^{(c_{\rm o})}}, \quad \forall c_{\rm o} \in \{\text{L,N}\} \quad (15)$$

where x is the link distance. For the i-layer receiver, the sum of total interference and noise is defined as

$$\mathcal{I}_i = \sum_{k\in\mathcal{K},c_{\rm o}\in\{\rm L,N\}} I_{ik}^{(c_{\rm o})} + \sigma^2 \quad (16)$$

where σ^2 is the noise power. Let us define $\varepsilon_{ij,\tau}^{(c)}(y)$ as the event that using the rule τ, a i-layer receiver associates to a j-layer transmitter, and their link distance is y and channel environment is $c \in \{\text{L,N}\}$. In the event of $\varepsilon_{ij,\tau}^{(c)}(y)$, the STP is defined using SINR as

$$p_{ij,\tau}^{(c)}(y) = \mathbb{P}\left[\text{SINR}_{ij}^{(c)}(y) > \beta_{ij} \mid \varepsilon_{ij,\tau}^{(c)}(y)\right], \quad (17)$$

$$\text{SINR}_{ij}^{(c)}(y) = P_j G_{ij}^{(c)} y^{-\alpha_{ij}^{(c)}} / \mathcal{I}_i. \quad (18)$$

Here, β_{ij} is the target SINR, which is related to the target transmission rate between a i-layer receiver and a j-layer transmitter. Based on the STP given event of $\varepsilon_{ij,\tau}^{(c)}(y)$ and the main link distance distribution, we analyze the STP and the ASE of the MAN in Section 4.

III. Interference Analysis of MANs

In this section, we analyze the Laplace transform of the interference in the MAN, which is generally required to analyze the network performance such as the STP, the ASE and the moments of the interference. From the property of the Laplace transform, the Laplace transform of the interference at a i-layer receiver $\mathcal{I}_i$ in (16) is given by

$$\mathcal{L}_{\mathcal{I}_i \mid \varepsilon_{ij,\tau}^{(c)}(y)}(s) = \exp(-s\sigma^2) \prod_{k\in\mathcal{K},c_{\rm o}\in\{\rm L,N\}} \mathcal{L}_{I_{ik}^{(c_{\rm o})} \mid \varepsilon_{ij,\tau}^{(c)}(y)}(s). \quad (19)$$

$$\mathcal{L}_{I_{ik}^{(c_o)}|\varepsilon_{ij,\tau}^{(c)}(y)}(s)=\exp\left[-2\pi\lambda_{k,\mathrm{Tx}}\int_{\max\left(\chi_{ij,k,\tau}^{(c,c_o)}(y),h_{ik}\right)}^{\infty}x\rho_{ik}^{(c_o)}(x)\left(1-\left(\frac{1}{1+\frac{sP_kx^{-\alpha_{ik}^{(c_o)}}}{m_{ik}^{(c_o)}}}\right)^{m_{ik}^{(c_o)}}\right)dx\right] \tag{20}$$

$$\mathcal{L}_{I_{ii}^{(c_o)}|\varepsilon_{ij,\tau}^{(c)}(y)}(s)=\begin{cases}\exp\left[2\pi\lambda_{i,\mathrm{Tx}}\sum_{n=1}^{\infty}\binom{-m_{ii}^{(c_o)}}{n}\left(\frac{sP_i}{m_{ii}^{(c_o)}}\right)^n\eta^{-g(n)}\Gamma\left(g(n),\eta\chi_{ij,i,\tau}^{(c,c_o)}(y)\right)\right],(c_o)=(\mathrm{L})\\ \exp\left[2\pi\lambda_{i,\mathrm{Tx}}\sum_{n=1}^{\infty}\binom{-m_{ii}^{(c_o)}}{n}\left(\frac{sP_i}{m_{ii}^{(c_o)}}\right)^n\left(-\frac{\left(\chi_{ij,i,\tau}^{(c,c_o)}\right)^{g(n)}}{g(n)}+\eta^{-g(n)}\Gamma\left(g(n),\eta\chi_{ij,i,\tau}^{(c,c_o)}(y)\right)\right)\right],(c_o)=(\mathrm{N})\end{cases} \tag{24}$$

In (19), $\mathcal{L}_{I_{ik}^{(c_o)}|\varepsilon_{ij,\tau}^{(c)}(y)}(s)$ is provided in the following lemma.

Lemma 2: In the case of $\varepsilon_{ij,\tau}^{(c)}(y)$, the Laplace transform of the interference from transmitters in the k-layer AN under the channel environment c_o is given by (20), shown at the top of this page, where $\chi_{ij,k,\tau}^{(c,c_o)}(y)$ is the minimum distance to the i-layer receiver from a transmitter (i.e., interfering node) in k-layer under channel c, given by

$$\chi_{ij,k,\tau}^{(c,c_o)}(y)=\begin{cases}R_{ij,k,a}^{(c,c_o)}(y) & \text{for } o=\mathrm{r},\\ 0 & \text{for } o=\mathrm{t},\end{cases} \tag{21}$$

where $R_{ij,k,a}^{(c,c_o)}(y)$ is defined in (8).

Proof: In the case of $\varepsilon_{ij,\tau}^{(c)}(y)$, the Laplace transform of the interference is then given by

$$\begin{aligned}&\mathcal{L}_{I_{ik}^{(c_o)}|\varepsilon_{ij,\tau}^{(c)}(y)}(s)\\&=\mathbb{E}\left[\prod_{\mathbf{x}\in\Phi_{ik,\mathrm{Tx}}^{(c_o)}}\exp\left\{-sP_kG_{ik}^{(c_o)}x^{-\alpha_{ik}^{(c_o)}}\right\}\,\middle|\,\varepsilon_{ij,\tau}^{(c)}(y)\right]\\&\overset{(a)}{=}\mathbb{E}_{\Phi_{ik,\mathrm{Tx}}^{(c_o)}}\left[\prod_{\mathbf{x}\in\Phi_{ik,\mathrm{Tx}}^{(c_o)}}\left(\frac{1}{1+\frac{sP_kx^{-\alpha_{ik}^{(c_o)}}}{m_{ik}^{(c_o)}}}\right)^{m_{ik}^{(c_o)}}\,\middle|\,\varepsilon_{ij,\tau}^{(c)}(y)\right].\end{aligned} \tag{22}$$

Here, (a) is obtained by averaging over the channel fading $G_{ik}^{(c_o)}$, which gives the moment-generating function (MGF) of Gamma distribution. Since the intensity function of the interference is $2\pi x\lambda_{k,\mathrm{Tx}}\rho_{ik}^{(c_o)}(x)$, the probability generating functional (PGFL) of PPP for function $f(x)$ is obtained as [26]

$$\begin{aligned}&\mathbb{E}_{\Phi_{ik,\mathrm{Tx}}^{(c_o)}}\left[\prod_{\mathbf{x}\in\Phi_{ik,\mathrm{Tx}}^{(c_o)}}f(\mathbf{x})\,\middle|\,\varepsilon_{ij,\tau}^{(c)}(y)\right]\\&=\exp\left(-2\pi\lambda_{k,\mathrm{Tx}}\int_{\max\left(\chi_{ij,k,\tau}^{(c,c_o)},h_{ik}\right)}^{\infty}x(1-f(x))\rho_{ik}^{(c_o)}(x)\,dx\right).\end{aligned} \tag{23}$$

When the node association rule $o=\mathrm{r}$ is used, there is no interferer with shorter distance than (8) to the receiver since a receiver selects the nearest or the strongest transmitter, and we get $\chi_{ij,k,\tau}^{(c,c_o)}(y)=R_{ij,k,a}^{(c,c_o)}(y)$ in (21). On the contrary, when $o=\mathrm{t}$, a transmitter selects a receiver, so the locations of the interferers are independent with the location of the main link transmitter, and we get $\chi_{ij,k,\tau}^{(c,c_o)}(y)=0$. From (22) and (23), we get the Laplace transform of the interference as (20). ■

Generally, the Laplace transform of the interference in (20) is not a closed-form since the integral cannot be removed. Compared with the non-closed-form expression, the closed-form expression takes advantages of computational speed, accuracy, and ease of use. In this work, we formulate the closed-form expression of (20) for the special case of of the interference from the transmitters in the same layer, i.e., $I_{ii}^{(c)}$ in the following corollary.

Corollary 1: The Laplace transform of the interference from transmitters in the i-layer to the receiver in the i-layer is given by (24), shown at the top of this page, when $sP_i\left(\chi_{ij,k,\tau}^{(c,c_o)}(y)\right)^{-\alpha_{ii}^{(c_o)}}<1$, where $g(n)=2-n\alpha_{ii}^{(c_o)}$, $\binom{-m_{ii}^{(c_o)}}{n}$ is binomial coefficient, and $\eta=-\sqrt{\mu\nu}\ln\left(1-\exp\left[-\frac{h_i^2}{2\xi^2}\right]\right)$.

Proof: From Lemma 2, the Laplace transform of $I_{ii}^{(\mathrm{L})}$ is given by

$$\begin{aligned}\mathcal{L}_{I_{ii}^{(\mathrm{L})}|\varepsilon_{ij,\tau}^{(c)}(y)}(s)&=\exp\left\{-2\pi\lambda_{i,\mathrm{Tx}}\int_{\chi_{ij,i,\tau}^{(c,\mathrm{L})}(y)}^{\infty}xe^{-\eta x}\right.\\&\quad\left.\times\left(1-\left(1/\left(1+\frac{sP_ix^{-\alpha_{ii}^{(\mathrm{L})}}}{m_{ii}^{(\mathrm{L})}}\right)\right)^{m_{ii}^{(\mathrm{L})}}\right)dx\right\}\\&\overset{(a)}{=}\exp\left\{2\pi\lambda_{i,\mathrm{Tx}}\int_{\chi_{ij,i,\tau}^{(c,\mathrm{L})}(y)}^{\infty}xe^{-\eta x}\right.\\&\quad\left.\times\sum_{n=1}^{\infty}\binom{-m_{ii}^{(\mathrm{L})}}{n}\left(\frac{sP_ix^{-\alpha_{ii}^{(\mathrm{L})}}}{m_{ii}^{(\mathrm{L})}}\right)^n dx\right\}\end{aligned} \tag{25}$$

$$\begin{aligned}&\overset{(b)}{=}\exp\left\{2\pi\lambda_{i,\mathrm{Tx}}\sum_{n=1}^{\infty}\binom{-m_{ii}^{(\mathrm{L})}}{n}\left(\frac{sP_i}{m_{ii}^{(\mathrm{L})}}\right)^n\eta^{n\alpha_{ii}^{(\mathrm{L})}-2}\right.\\&\quad\left.\times\int_{\eta\chi_{ij,i,\tau}^{(c,\mathrm{L})}(y)}^{\infty}t^{1-n\alpha_{ii}^{(\mathrm{L})}}e^{-t}dt\right\},\end{aligned} \tag{26}$$

where (a) follows from the Taylor series $(1+x)^{-m}=\sum_{n=0}^{\infty}\binom{-m}{n}(x)^n$, which is convergent for $|x|<1$, so,

(25) is convergent for $sP_i x^{-\alpha_{ii}^{(c_o)}} < 1$, and (b) follows from integration by substitution $\eta x = t$. In (26), by definition of the upper incomplete gamma function $\Gamma(x,y) = \int_y^\infty t^{x-1}e^{-t}dt$, we get the upper part of (24). In a similar way, the Laplace transform of the interference in the NLoS environment, $I_{ii}^{(\mathrm{N})}$, is given by

$$\begin{aligned}
&\mathcal{L}_{I_{ii}^{(\mathrm{N})}|\varepsilon_{ij,\tau}^{(c)}(y)}(s) \\
&= \exp\left[2\pi\lambda_{i,\mathrm{Tx}}\int_{\chi_{ij,i,\tau}^{(c,\mathrm{N})}(y)}^{\infty} x(1-e^{-\eta x}) \right. \\
&\quad \left. \times \sum_{n=1}^{\infty}\binom{-m_{ii}^{(\mathrm{N})}}{n}\left(\frac{sP_i x^{-\alpha_{ii}^{(\mathrm{N})}}}{m_{ii}^{(\mathrm{N})}}\right)^n dx\right] \\
&= \exp\left[2\pi\lambda_{i,\mathrm{Tx}}\sum_{n=1}^{\infty}\binom{-m_{ii}^{(\mathrm{N})}}{n}\left(\frac{sP_i}{m_{ii}^{(\mathrm{N})}}\right)^n \frac{\left(\chi_{ij,i,\tau}^{(c,\mathrm{N})}(y)\right)^{2-n\alpha_{ii}^{(\mathrm{N})}}}{\left(n\alpha_{ii}^{(\mathrm{N})}-2\right)}\right. \\
&\quad \left. -2\pi\lambda_{i,\mathrm{Tx}}\int_{\chi_{ij,i,\tau}^{(c,\mathrm{N})}(y)}^{\infty} xe^{-\eta x}\sum_{n=1}^{\infty}\binom{-m_{ii}^{(\mathrm{N})}}{n}\left(\frac{sP_i x^{-\alpha_{ii}^{(\mathrm{N})}}}{m_{ii}^{(\mathrm{N})}}\right)^n dx\right]
\end{aligned} \tag{27}$$

From (27), we get the lower part of (24). ∎

IV. Performance Analysis of MANs

In this section, we analyze the STP and the ASE of MAN based on the Laplace transform of the interference. In addition, we derive the upper bound of the optimal density that maximizes the STP and the ASE.

A. STP and ASE Analysis

We define the STP under the event $\varepsilon_{ij,\tau}^{(c)}(y)$ in (17). In this subsection, we show the STP of the MAN, which is the expectation of the STP of the node in the MAN. We first obtain the STP under the event $\varepsilon_{ij,\tau}^{(c)}(y)$, by using the Laplace transform of the interference. Then, using the PDF of the main link distance and the association probability, we obtain the average of the STP in the MAN. In addition, we derive the ASE, where the definition is given as the sum of the maximum average data rates per unit bandwidth per unit area for a specified bit error rate [40], [41]. Here, we assume the number of communication links in the unit area depends on the number of the transmitters and the number of the receivers for $o = \mathrm{t}$ and $o = \mathrm{r}$, respectively. Therefore, when $o = \mathrm{r}$, we define the ASE as the data rate multiplied with the density of the receivers. On the contrary, when $o = \mathrm{t}$, we define the ASE as the data rate multiplied with the density of the transmitters. Here, the data rate is $R_{ij} = \log(1+\beta_{ij})$ when the communication succeeds, and $R_{ij} = 0$ when the communication is failed. In Theorem 1, we derive the STP and the ASE of the MAN. Note that in Theorem 1, the k-layer denotes the layer of the association subject, which is the layer of receivers for $o = \mathrm{r}$ and that of transmitters for $o = \mathrm{t}$.

Theorem 1: In the MAN, the STP and the ASE of the network is given by

$$\mathcal{P}_{\mathrm{MAN},\tau} = \begin{cases} \sum_{i\in\mathcal{K}} \frac{\lambda_{i,\mathrm{Rx}}}{\lambda_{T,\mathrm{Rx}}}\mathcal{P}_{i,\tau} & \text{for } o = \mathrm{r}, \\ \sum_{i\in\mathcal{K}} \frac{\lambda_{i,\mathrm{Tx}}}{\lambda_{T,\mathrm{Tx}}}\mathcal{P}_{i,\tau} & \text{for } o = \mathrm{t}, \end{cases} \tag{28}$$

$$\mathcal{S}_{\mathrm{MAN},\tau} = \sum_{i\in\mathcal{K}} \mathcal{S}_{i,\tau}. \tag{29}$$

where $\mathcal{P}_{k,\tau}$ and $\mathcal{S}_{k,\tau}$ are the STP and the ASE of k-layer AN for τ, given as

$$\mathcal{P}_{k,\tau} = \begin{cases} \sum_{j\in\mathcal{K},c\in\{\mathrm{L},\mathrm{N}\}} f_{\mathcal{P}}(k,j,c,\tau) & \text{for } o = \mathrm{r}, \\ \sum_{i\in\mathcal{K},c\in\{\mathrm{L},\mathrm{N}\}} f_{\mathcal{P}}(i,k,c,\tau) & \text{for } o = \mathrm{t}, \end{cases} \tag{30}$$

$$\mathcal{S}_{k,\tau} = \begin{cases} \sum_{j\in\mathcal{K},c\in\{\mathrm{L},\mathrm{N}\}} \lambda_{j,\mathrm{Rx}} R_{kj} f_{\mathcal{P}}(k,j,c,\tau) & \text{for } o = \mathrm{r}, \\ \sum_{i\in\mathcal{K},c\in\{\mathrm{L},\mathrm{N}\}} \lambda_{j,\mathrm{Tx}} R_{ik} f_{\mathcal{P}}(i,k,c,\tau) & \text{for } o = \mathrm{t}. \end{cases} \tag{31}$$

where $R_{ij} = \log_2(1+\beta_{ij})$ and $f_{\mathcal{P}}(i,j,c,\tau)$ is given as

$$f_{\mathcal{P}}(i,j,c,\tau) = \mathcal{A}_{ij,\tau}^{(c)} \int_{h_{ij}}^{\infty} p_{ij,\tau}^{(c)}(y) f_{Y_{ij,\tau}^{(c)}}(y)dy. \tag{32}$$

Here, $p_{ij,\tau}^{(c)}(y)$ is presented as

$$p_{ij,\tau}^{(c)}(y) = \sum_{n=0}^{m^{(c)}-1} \frac{(-s)^n}{n!}\frac{d^n}{ds^n}\mathcal{L}_{\mathcal{I}_i|\varepsilon_{ij,\tau}^{(c)}(y)}(s)\Big|_{s=l_{ij}^{(c)}(y)}, \tag{33}$$

$$l_{ij}^{(c)}(y) = \frac{m_{ij}^{(c)}\beta_{ij}}{P_j y^{-\alpha_{ij}^{(c)}}}, \tag{34}$$

where $\mathcal{L}_{\mathcal{I}_i|\varepsilon_{ij,\tau}^{(c)}(y)}(s)$ is in (19).

Proof: From (17) and (18), the STP for the event $\varepsilon_{ij,\tau}^{(c)}(y)$ is given by

$$\begin{aligned}
p_{ij,\tau}^{(c)}(y) &= \mathbb{P}\left[\frac{P_j y^{-\alpha_{ij}^{(c)}} G_{ij}^{(c)}}{\mathcal{I}_i} > \beta_{ij} \,\middle|\, \varepsilon_{ij,\tau}^{(c)}(y)\right] \\
&= \mathbb{P}\left[G_{ij}^{(c)} > \frac{\beta_{ij}\mathcal{I}_i}{P_j y^{-\alpha_{ij}^{(c)}}} \,\middle|\, \varepsilon_{ij,\tau}^{(c)}(y)\right] \\
&\overset{(a)}{=} \mathbb{E}\left[1 - \frac{1}{\Gamma(m_{ij}^{(c)})}\gamma\left(m_{ij}^{(c)}, \frac{m_{ij}^{(c)}\beta_{ij}}{P_j y^{-\alpha_{ij}^{(c)}}}\mathcal{I}_i\right) \,\middle|\, \varepsilon_{ij,\tau}^{(c)}(y)\right] \\
&\overset{(b)}{=} \mathbb{E}_{\mathcal{I}_i}\left[\sum_{n=0}^{m^{(c)}-1}\frac{(s\mathcal{I}_i)^n}{n!}\exp\left(-s\mathcal{I}_i\right) \,\middle|\, \varepsilon_{ij,\tau}^{(c)}(y)\right]\Bigg|_{s=l_{ij}^{(c)}(y)}
\end{aligned} \tag{35}$$

where (a) follows from the Nakagami-m fading $G_{ij}^{(c)}$, (b) follows from the Gamma distribution of channel gain and the property of lower incomplete Gamma function. Notice that we derive (34) from (b). Using following property of the Laplace transform, we obtain (33).

$$\begin{aligned}
&\mathcal{L}_{\mathcal{I}_i}(s) = \mathbb{E}_{\mathcal{I}_i}\left[\exp\left(-s\mathcal{I}_i\right)\right], \\
&\mathbb{E}_{\mathcal{I}_i}\left[(-\mathcal{I}_i)^n \exp\left(-s\mathcal{I}_i\right)\right] = \frac{d^n}{ds^n}\mathcal{L}_{\mathcal{I}_i}(s).
\end{aligned} \tag{36}$$

Therefore, by averaging $p_{ij,\tau}^{(c)}(y)$ in (35) over the main link distance $f_{Y_{ij,\tau}^{(c)}}(y)$ considering the association probability to each layer $\mathcal{A}_{ij,\tau}^{(c)}$ in Lemma 1, we can present probability that transmission succeed when the receiver layer i and the transmitter layer j is involved, i.e., $f_{\mathcal{P}}(i,j,c,\tau)$, in (32). Based on $f_{\mathcal{P}}(i,j,c,\tau)$, when the receiver-oriented association case, the STP of the k-layer associated with transmitter layers in the MAN, i.e., $i \in \mathcal{K}$, is given as (30). By a similar process, we can also obtain the STP of the k-layer AN of the transmitter-oriented association case. Furthermore, the ASE is defined as the total date rate successfully transmitted in unit area [40], [41]. By the definition, for the receiver-oriented association case, we can present the ASE of k-layer receivers, associating to j-layer transmitters as

$$\mathcal{S}_{kj,\tau} = \lambda_{k,\mathrm{Rx}} \log_2(1+\beta_{kj}) f_{\mathcal{P}}(k,j,c,\tau) \tag{37}$$

where β_{ij} is the target SINR of the j-layer transmitter to the i-layer receiver. Here, as it is the receiver-oriented associate case, the communication links are formed by the receivers, so the average number of communication links in the network per unit area becomes the density of the receivers, i.e., $\lambda_{j,\mathrm{Rx}}$, which is used in (37). Finally, as the k-layer receiver can associate to each layer with the association probabilities, we obtain the ASE of the k-layer AN as (31). By a similar process, we can also obtain the ASE of the k-layer AN for the transmitter-oriented association case as (31). ∎

The STP and the ASE have multiple integral that makes evaluation hard. However, the integral in the Laplace transform can be removed under the certain condition, which is explained in the following remark.

Remark 1: In Lemma 3, the Laplace transform of the interference from the same layer of AN can be replaced with (24) when $\tau = \mathrm{rs}$, $\frac{m_{ij}^{(c)}}{m_{ii}^{(c_\mathrm{o})}}\beta_{ij} < 1$, for all $c, c_\mathrm{o} \in \{\mathrm{L},\mathrm{N}\}$ and $B_k = P_k$, since the conditions in Corollary 1 are satisfied.

Proof: In the event of $\varepsilon_{ij,\tau}^{(c)}(y)$, using the node association $\tau = \mathrm{rs}$, $\chi_{ij,k,\tau}^{(c,c_\mathrm{o})}(y) = R_{ij,k,a}^{(c,c_\mathrm{o})}(y)$, hence, if $sP_i\left(\chi_{ij,k,\tau}^{(c,c_\mathrm{o})}(y)\right)^{-\alpha_{ii}^{(c_\mathrm{o})}} < 1$ holds for $R_{ij,k,a}^{(c,c_\mathrm{o})}(y) \le x$, the condition in Lemma 3 always holds. In (34), by replace s with $l_{ij}^{(c)}$ for the Laplace transform, we obtain $l_{ij}^{(c)}(y)P_i x^{-\alpha_{ii}^{(c_\mathrm{o})}} = \beta_{ij}\frac{P_i x^{-\alpha_{ii}^{(c_\mathrm{o})}} m_{ij}^{(c)}}{P_j y^{-\alpha_{ij}^{(c)}} m_{ii}^{(c_\mathrm{o})}} < \beta_{ij}\frac{m_{ij}^{(c)}}{m_{ii}^{(c_\mathrm{o})}}$. Therefore, if $\beta_{ij}\frac{m_{ij}^{(c)}}{m_{ii}^{(c_\mathrm{o})}} < 1$, condition $sP_i\left(\chi_{ij,k,\tau}^{(c,c_\mathrm{o})}(y)\right)^{-\alpha_{ii}^{(c_\mathrm{o})}} < 1$ in Corollary 1 is satisfied. ∎

Our performance analysis for the fixed altitude MAN can be extended for the MAN that has UAV with random altitude, e.g., uniform altitude as in [20]. In the following remark, we introduce how the analysis can be extended.

Remark 2: The performance analysis of the MAN can be extended to the MAN with UAV that has random altitude with the following procedure:

- the STP of i-layer $f_{\mathcal{P}}(i,j,c,\tau)$ modified to be the expectation of the main link distance x and the altitude of the receiver layer h_i;
- the CCDF and the PDF of the nearest node distance $\bar{F}_{V_{ik,o}^{(c_\mathrm{o})}}$ and $f_{V_{ik,o}^{(c_\mathrm{o})}}$, that are used for the main link distance distribution and the association probability, are the expectation of the altitude of the transmitter layer h_k for given receiver layer altitude h_i; and
- the Laplace transform of the interference from the k-layer to the i-layer $\mathcal{L}_{I_{ik}^{(c_\mathrm{o})}|\varepsilon_{ij,\tau}^{(c)}(y)}(s)$, that used for the STP under event of $\varepsilon_{ij,\tau}^{(c)}(y)$, is expectation of the altitude of the transmitter layer h_k given receiver layer altitude h_i.

Note that as the distribution of altitudes are considered, the expectations with respect to the receiver and the transmitter layers requires, that makes the analysis and the numerical evaluation complex, while the performance compared with the fixed altitude has little difference as shown in Section V.

B. Upper Bound of Optimal Density

In the design of the MAN, it is important to optimize the densities of transmitters in order to maximize the STP and the ASE. However, due to the non-closed-form expressions of the STP and the ASE, we cannot present the optimal transmitter density in a closed form. Hence, it is required to use a search algorithm such as the exhaustive search algorithm, which consumes considerable computational resource and time due to the complicated expression of the STP and the ASE. Therefore, in the following Corollary 2, we provide the upper bound of the optimal transmitter density, which can reduce the computational complexity of the optimal density search algorithm by restricting the search range. We use k that act as a receiver layer when $o = \mathrm{r}$, and act as a transmitter layer when $o = \mathrm{t}$.

Corollary 2: When the channel coefficient is $m_{ij}^{(\mathrm{L})} = m_{ij}^{(\mathrm{N})} = 1$ for all $i,j \in \mathcal{K}$, the upper bound of the optimal transmitter density in the j-layer that maximizes the STP, $\lambda_{j,\mathrm{Tx}}^{b,\mathcal{P}_{k,\tau}}$, and that maximizes the ASE, $\lambda_{j,\mathrm{Tx}}^{b,\mathcal{S}_{k,\tau}}$, of the k-layer are respectively given by

$$\lambda_{j,\mathrm{Tx}}^{b,\mathcal{P}_{k,\tau}} = \begin{cases} \frac{1}{2\pi\epsilon_{kj}} & \text{for } o = \mathrm{r}, \\ 0 & \text{for } o = \mathrm{t}, \end{cases} \tag{38}$$

$$\lambda_{j,\mathrm{Tx}}^{b,\mathcal{S}_{k,\tau}} = \begin{cases} \dfrac{1}{2\pi\epsilon_{kj}} & \text{for } o = \mathrm{r}, \\ 0 & \text{for } o = \mathrm{t} \text{ and } k \neq j, \\ \max_{i\in\mathcal{K}}\left[\frac{1}{2\pi\epsilon_{ik}}\right] & \text{for } o = \mathrm{t} \text{ and } k = j. \end{cases} \tag{39}$$

where ϵ_{ij} is

$$\epsilon_{ij} = \int_{h_{ij}}^{\infty} x\left(1 - \frac{\rho_{ij}^{(\mathrm{L})}(x)}{1+\beta_{ij}h_{ij}^{\alpha_{ij}^{(\mathrm{L})}}x^{-\alpha_{ij}^{(\mathrm{L})}}} - \frac{\rho_{ij}^{(\mathrm{N})}(x)}{1+\beta_{ij}h_{ij}^{\alpha_{ij}^{(\mathrm{L})}}x^{-\alpha_{ij}^{(\mathrm{N})}}}\right)dx. \tag{40}$$

Proof: See Appendix A. ∎

Note that when $o = \mathrm{r}$, the optimal transmitter density exists for both the ASE and the STP due to the trade-off: as the transmitter density increases, the main link distance becomes shorter and the number of communication links in the network increases, while the interference becomes larger. However, when $o = \mathrm{t}$, as the density of transmitters increases,

TABLE II
SIMULATION PARAMETERS

Parameter	Value	Parameter	Value
$(m^{(\mathrm{L})}, m^{(\mathrm{N})})$	(1, 1)	(μ, ν, ξ)	$(0.5,\ 3\times10^{-4},\ 20)$
$(\alpha^{(\mathrm{L})}, \alpha^{(\mathrm{N})})$	(2.5, 3.5)	(ι, κ)	(12.0910, 0.1139)
a	$a = \mathrm{s}$	β	0.7
(B_j, P_j)	1	Receiver layer	$0, i$
σ^2	0	Transmitter layer	j, k

the main link distance remains unchanged (since it depends on the receiver distribution, not on the transmitter distribution), while the interference is getting larger. Hence, when $o = \mathrm{t}$, the STP keeps decreasing with the transmitter density, so the optimal transmitter density becomes zero.

From Corollary 2, we can also see the following tendency of the upper bound.

Corollary 3: The upper bound of the optimal transmitter densities $\lambda_{j,\mathrm{Tx}}^{b,\mathcal{P}_{i,\tau}}$ and $\lambda_{j,\mathrm{Tx}}^{b,\mathcal{S}_{i,\tau}}$, are non-increasing function of h_{ij} under the conditions of $\beta_{ij} h_{ij}^{\alpha^{(\mathrm{L})}} > 1$ and $h_{ij} > 1$, since ϵ_{ij} increases with h_{ij}.

Proof: See Appendix B. ∎

Note that the condition $\beta_{ij} h_{ij}^{\alpha^{(\mathrm{L})}} > 1$ and $h_{ij} > 1$ are conditions, which are generally satisfied in UAV communications. From Corollary 3, we can see that as the altitude difference between the transmitter and the receiver h_{ij} increases, the optimal transmitter density bound becomes smaller, which will be almost zero for large altitude difference.

V. NUMERICAL RESULTS

In this section, we present the STP and the ASE of the MAN for the receiver-oriented and the transmitter-oriented association cases. For the numerical results, we consider the interference-limited environment, i.e., $\sigma^2 = 0$, the same path loss exponent and fadings, i.e., $\alpha_{ij}^{(c)} = \alpha^{(c)}$ and $m_{ij}^{(c)} = m^{(c)}$ in order to clarify the results. We use the ground layer, i.e., 0-layer, and i-layer as receivers' layer, j-layer and k-layer as the transmitters' layers, and omit the subscripts Rx and Tx for the simplicity, e.g., $\lambda_0 = \lambda_{0,\mathrm{Rx}}$ and $\lambda_j = \lambda_{j,\mathrm{Tx}}$. Furthermore, we omit the subscript in the total transmitter density, i.e., $\lambda_j + \lambda_k = \lambda_T$ instead of $\lambda_{T,\mathrm{Tx}}$. Simulation parameters for our numerical results summarized in Table. II, where Figs. 3 and 4 uses $m^{(\mathrm{L})} = 3$.

A. Receiver-Oriented Association Case

In this subsection, we show the STP of the MAN when the receiver-oriented association is considered. The ASE results are not provided for the receiver-oriented association case since the ASE is a multiplication of the STP with the receiver density, which gives the same tendency with the STP. To show the effects of network parameters on the performance more clearly, we first show the performance for a single layer AN case in Figs. 3-6 and 8, then provide the performance for a two layer MAN case in Fig. 7.

Figure 3 shows the STP of the single layer AN (i.e., the j-layer) as a function of the altitude of the layer h_j for different

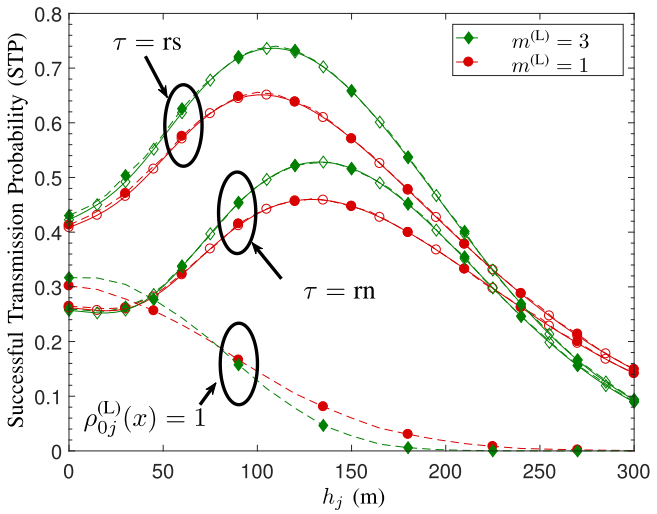

Fig. 3. STP of the single layer AN according to the transmitter altitude h_j with different LoS coefficient $m^{(\mathrm{L})}$ when $\lambda_j = 10^{-5}$, $o = \mathrm{r}$. The STP of the strongest node association $a = \mathrm{s}$ outperforms nearest node association $a = \mathrm{n}$. The STP first increases and then decreases with the height, while this tendency is not observed when $\rho_{0j}^{(\mathrm{L})}(x) = 1$.

values of channel coefficient $m^{(\mathrm{L})} = \{1, 3\}$ and two node association rules, i.e., the strongest power ($\tau = \mathrm{rs}$) and the nearest distance ($\tau = \mathrm{rn}$) associations. Here, the density of the transmitters is $\lambda_j = 10^{-5}$ [nodes/m^2]. The LoS probability in (2) is used for this figure, and we also provide the results with $\rho_{0j}^{(\mathrm{L})} = 1$ (i.e., the case that always assumes LoS link) to show the effect of the LoS probability consideration. Simulation results are obtained from Monte Carlo simulation which are presented by the dashed lines with filled markers, while analysis results are presented by the solid lines with unfilled markers, which fit well with the simulation results.

From Fig. 3, we observe the tendency of the performance according to the altitude: as the altitude of the AN increases, the STP and the ASE first increase and then decrease, that gives the optimal altitude of the AN, which also appears in Figs. 4-6 and Figs. 8-10. As the UAV altitude increases, the LoS probabilities of the main link as well as the interfering link increase, which means both the main link and the interfering link have stronger channel gain. Since the main link has smaller distance, the LoS probability of the main link increases more rapidly than that of the interfering links. Therefore, the STP and the ASE first increase. However, after a certain value of the altitude, due to the increased main link distance, the STP and the ASE decrease. Note that as the LoS probability is not changed when $\rho_{0j}^{(\mathrm{L})} = 1$, the STP only decreases due to the main link distance increases with the altitude.

In addition, we observe the effect of the LoS coefficient $m^{(\mathrm{L})}$ on the STP, which gives higher STP at low altitude region (e.g., $h_j < 200$) and gives lower STP at high altitude region (e.g., $h_j > 230$). For the Nakagami-m fading, the larger coefficient $m^{(c)}$ gives less chance to have the smaller channel gain. At the low altitude region, the main link is mostly LoS while the interference is NLoS that gives the higher SINR with the larger LoS coefficient $m^{(\mathrm{L})}$. On the contrary, at the

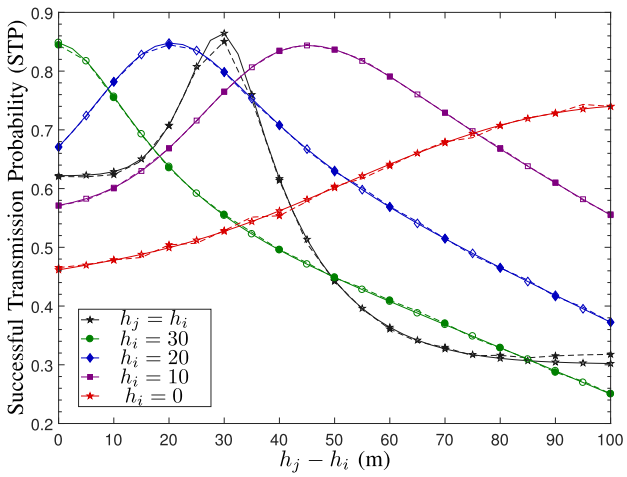

Fig. 4. STP of the single layer AN according to the difference of altitude between layers $h_j - h_i$ with different receiver altitudes h_i when $\lambda_j = 10^{-5}$ and $\tau =$ rs. STP first increases then decreases with the altitude difference $h_j - h_i$, and the optimal $h_j - h_i$ decreases as the altitude of the receiver layer h_i increases.

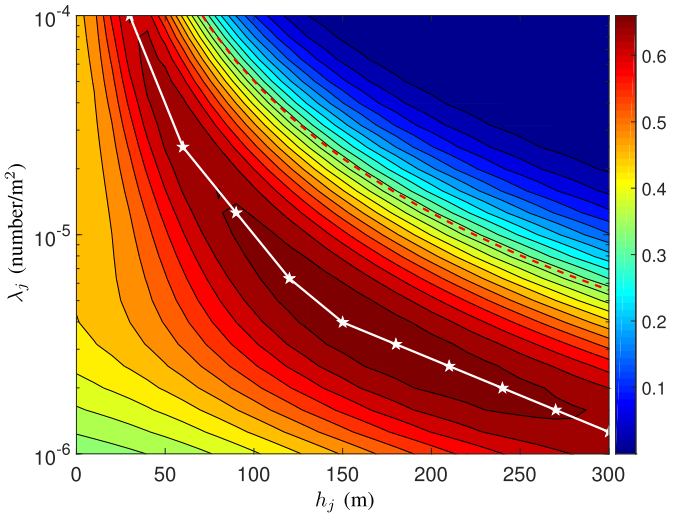

Fig. 5. STP of the single layer AN as functions of the transmitter density λ_j and the transmitter altitude h_j when $\tau =$ rs. A solid line with stars presents the optimal density and a dotted line presents the upper bound of the optimal density.

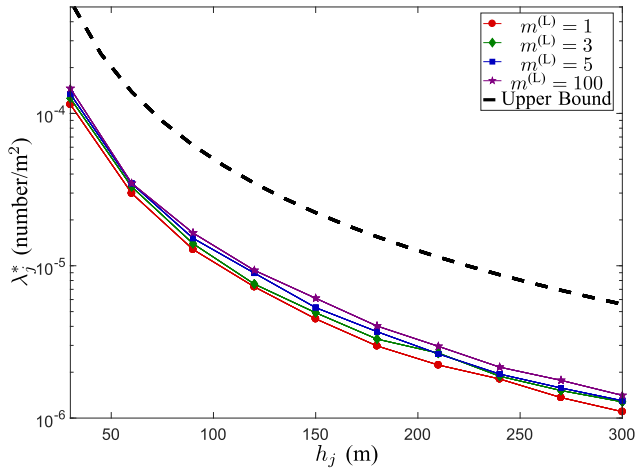

Fig. 6. Optimal density of the single layer AN according to the altitude with different LoS coefficient $m^{(\mathrm{L})}$.

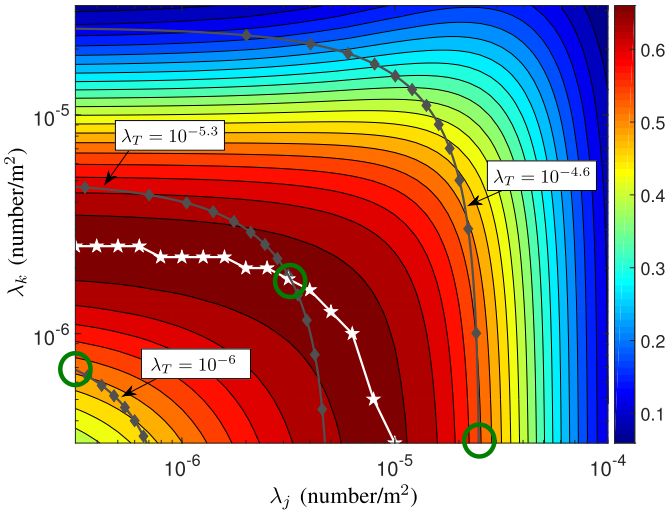

Fig. 7. STP of the two layer MAN as functions of the j-layer transmitter density λ_j and the k-layer transmitter density λ_k when $h_j = 100$, $h_k = 200$, and $\tau =$ rs. A line with stars presents the optimal j-layer transmitter density and a line with diamonds presents the area that has the same total density λ_T.

high altitude region, the interference has more LoS links which gives the lower SINR with the larger LoS coefficient $m^{(\mathrm{L})}$.

Figure 4 depicts the STP of the single layer AN[4] as a function of the altitude difference between the j-layer (i.e., transmitter layer) and the i-layer (i.e., receiver layer), $h_j - h_i$, for different altitudes of the i-layer, $h_i = \{0, 10, 20, 30\}$, when $h_j > h_i$. Here, the strongest power association ($\tau =$ rs) is used and $\lambda_j = 10^{-5}$. The simulation results are presented by the dashed lines with filled markers, while analysis results are presented by the solid lines with unfilled markers. For the analysis results, we use Lemma 2 for $h_i = \{0, 10, 20, 30\}$ and Corollary 1 for the case of $h_i = h_j$, and show that analysis results match well with the simulation results. Note that since the infinite summation (i.e., $\sum_{n=1}^{\infty}$) in Corollary 1 cannot be realized, we use the truncated summation $\sum_{n=1}^{30}$ instead in the analysis results.

From Fig. 4, we observe that the optimal altitude difference $(h_j - h_i)^*$ that maximizes the STP exists and decreases with h_i. Considering $h_i = h_j$, which is the same with the communication between nodes in the same layer, optimal altitude of layer h_i exist since the LoS probability of the main link and the interfering links increases with h_i. At low altitude region (e.g., $h_i = 0$), the channel is mostly NLoS, at high altitude region (e.g., $h_i = 100$), contrary, the channel is mostly LoS. When $h_i = 30$, the LoS probability is high when the smaller horizontal distance is considered, therefore, the main link is under LoS channel whereas the interfering links are under NLoS channel, that gives the higher STP compared with the low and high altitude.

[4]Even though we use two ANs, i and j-layer, we regard it as the single layer AN since only one layer acts as the transmitter and the receiver.

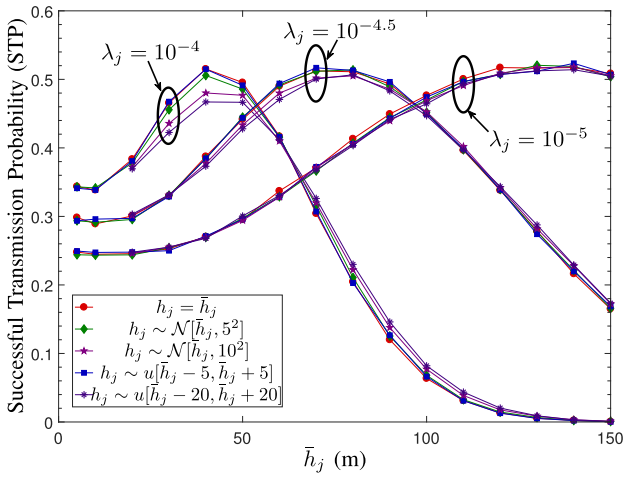

Fig. 8. STP of the single layer AN according to the mean altitude $\bar{h}_j$ with different altitude distributions and density of the j-layer λ_j, when the ground receiver altitude is $h_0 = 0$.

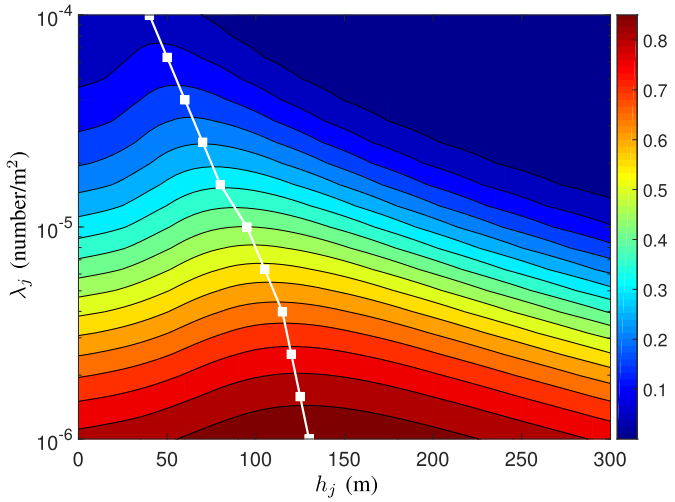

Fig. 9. STP of the single layer AN as functions of the transmitter density λ_j and the transmitter altitude h_j when $\tau =$ ts. A solid line with squares presents the optimal altitude.

Figure 5 shows the STP of the single layer AN as functions of the transmitter density λ_j and the transmitter altitude h_j when $\tau =$ rs. We present the optimal density λ_j^* that maximizes the STP using a solid line with stars and the upper bound of the optimal density, obtained from Corollary 2, as a dashed line. For the receiver-oriented association case, as the UAV density increases, the STP and the ASE first increase and then decrease, that gives the optimal density of the AN, which also appears in Figs. 5-7. As the UAV density increases, the distances of the main link, as well as the interfering links, decrease, and the LoS probabilities of both the main and the interfering links decrease that increase the LoS probability of the main and interfering links. Since the main link distance is smaller than the interfering links, the LoS probability rapidly increases, therefore, the STP and the ASE first increase. However, after a certain value of the UAV density, due to the increased interference, the STP and the ASE decrease.

Furthermore, by comparing the optimal density and the upper bound of the optimal density, we notice that their trends

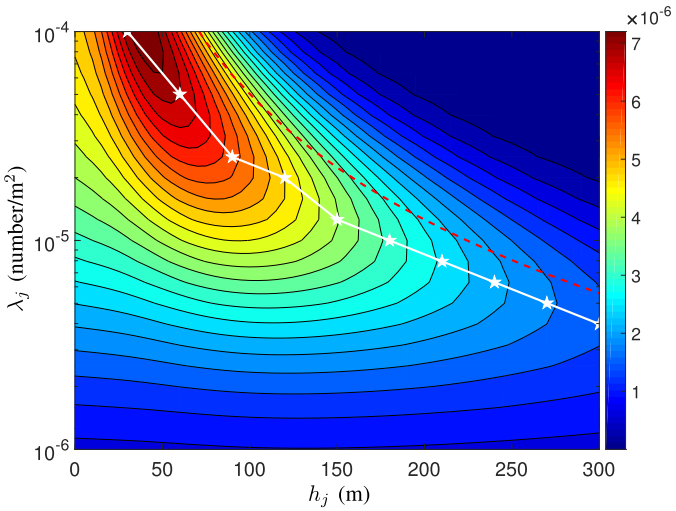

Fig. 10. ASE of the single layer AN as functions of the transmitter density λ_j and the transmitter altitude h_j when $\tau =$ ts. A solid line with stars presents the optimal density and a dotted line presents the upper bound of the optimal density.

according to the altitude h_j are similar. Specifically, both the optimal density and its upper bound decrease with the altitude h_j as proven in Corollary 3. Figure 6 additionally shows the optimal density of the single layer AN according to the altitude with different LoS coefficient $m^{(\mathrm{L})}$. The dashed line presents the upper bound of the optimal density when $m^{(\mathrm{L})} = m^{(\mathrm{N})} = 1$. In this figure, we observe Corollary 2 and Corollary 3 empirically applied to the case when $m^{(\mathrm{L})} > 1$. Since as the signal and the interference largely affected by the path loss and the LoS probablity when the interference limited environment is considered, the optimal densities are similar for different LoS coefficient $m^{(\mathrm{L})}$. Although the difference between the optimal density and its upper bound is not small, the upper bound can play an important to find the optimal density by restricting the searching range, e.g., exhaustive searching starting from the upper bound.

Figure 7 shows the STP of the two layer MAN as functions of the density of j-layer transmitters λ_j and the density of k-layer transmitters λ_k, when $h_j = 100$, $h_k = 200$, and $\tau =$ rs. The line marked with stars shows the optimal transmitter density of the k-layer λ_k^* for different values of λ_j. We can see that λ_k^* decreases as λ_j increases. This is because the larger interference from the j-layer that makes the density of other interfering layer to decrease (i.e., k-lyaer), for the optimal density. The lines marked with diamonds show the cases of having the given values of the total density, i.e., $\lambda_j + \lambda_k = \lambda_T$, and the points of circles show the optimal densities $(\lambda_j, \lambda_k)^*$ for each cases of λ_T. We can see that when λ_T is large (e.g., $\lambda_T = 10^{-4.6}$), having all transmitters in the layer with lower altitude (i.e., the j-layer) can achieve higher STP, while for small λ_T (e.g., $\lambda_T = 10^{-6}$), having all transmitters in the layer with higher altitude (i.e., the k-layer) achieves higher STP. However, when λ_T is neither large or small, e.g., $\lambda_T = 10^{-5.3}$, having transmitters in multiple layers, i.e., both j and k-layers can be better in terms of the STP.

In Fig. 8, we compare the simulation results of STP of the AN for the cases of the fixed altitude $\bar{h}_j$, the normal

distribution altitude (i.e., $h \sim \mathcal{N}[\bar{h}_j, \sigma^2]$), and the uniform distribution altitude (i.e., $h \sim u[\bar{h}_j - \sigma, \bar{h}_j + \sigma]$). As shown in this figure, *the trends of STP with random altitudes are similar to that with fixed altitude*, especially when the range or variance of the altitude is small like the cases with $\sigma = 5$. The values of STP for all cases become even more similar as the UAV density decreases and the mean altitude increases. Note that the difference between the random altitude MAN and the fixed altitude MAN increases as the density increases and the altitude decreases. Furthermore, even though the range or the variance is high, by dividing the 3D segment of the AN, the MAN can approximate the AN with sufficient accuracy. Therefore, from those results, we can see that the performance of the MAN with fixed altitude can be an approximated performance of the MAN with random altitudes.

B. Transmitter-Oriented Association Case

In this subsection, we show the STP and the ASE of the MAN when the transmitter-oriented association and the ground receiver in the 0-layer with density $\lambda_0 = 10^{-5}$ is considered. We show the performance for a single layer AN case in Figs. 9 and 10, and then provide the performance for a two layer MAN case in Figs. 11 and 12.

Figures 9 and 10 show the STP and ASE of the single layer AN as functions of the transmitter density λ_j and their altitude h_j when $\tau =$ ts. The solid line with squares presents the optimal altitudes h_j^* that maximizes STPs (in Fig. 9) and the solid line with stars presents the optimal density λ_j^* that maximizes ASE (in Fig. 10) for different values of λ_j. The dashed line in Fig. 10 presents the upper bound of the optimal transmitter density, obtained from Corollary 2. For the transmitter-oriented association case, as the UAV density increases, the ASE first increases then decreases, that gives the optimal density of the AN that maximizes the ASE, which also appears in Fig. 11. However, the STP keep decreases, that gives the optimal density of the AN that maximizes the STP zero. As the UAV density increases, the main link distance does not decrease with the UAV (i.e., transmitter) density. Therefore, increasing UAV density only increases the interference, which makes the STP decreases. On the other hand, the number of communication links in the MAN increases with the UAV density. Hence, then ASE increases for small UAV density, but decrease for large UAV density due to the larger interference.

From the discussion on the results in Fig. 9, we can readily guess that in the transmitter-oriented association case, the main link distance remains the same while the interference increases as the transmitter densities of each layer increase in MAN. Hence, the numerical results for the STP of the two layer MAN are not provided in this paper as the optimal transmitter densities of each layer are obviously zero.

Figure 11 show the ASE of the two layer MAN as functions of the j-layer transmitter density λ_j and the k-layer transmitter density λ_k when $h_j = 100$, $h_k = 200$. The line marked with stars shows the optimal transmitter density of the k-layer λ_k^* for different values of λ_j. The lines marked with diamonds show the cases of having given values of the total transmitter density, i.e., $\lambda_j + \lambda_k = \lambda_T$, and the optimal density pairs $(\lambda_j, \lambda_k)^*$ is marked with circles for different λ_T. From Fig. 11, we can see that when λ_T is large (e.g., $\lambda_T = 10^{-5}$ and $\lambda_T = 10^{-4.5}$), $\lambda_j^* > 0$ and $\lambda_k^* = 0$. However, when λ_T is small (e.g., $\lambda_T = 10^{-6}$), $\lambda_k^* > 0$ and $\lambda_j^* = 0$.

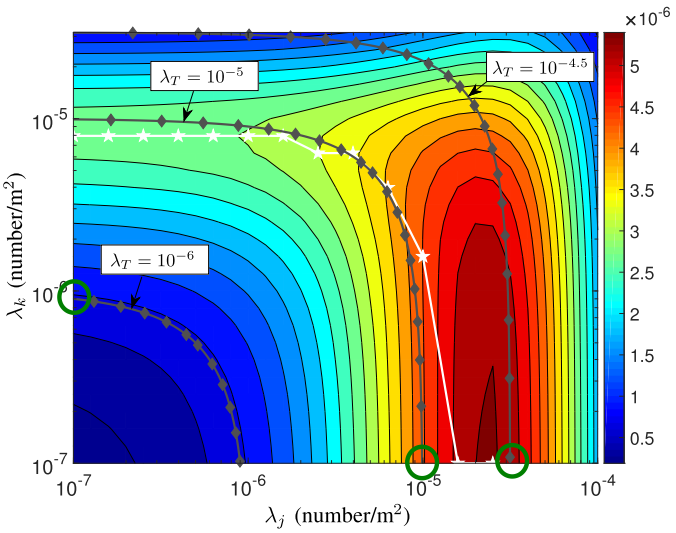

Fig. 11. ASE of the two layer MAN as functions of the j-layer transmitter density λ_j and the k-layer transmitter density λ_k when $h_j = 100$, $h_k = 200$, and $\tau =$ ts. A line with stars presents the optimal j-layer transmitter density and a line with diamonds presents the area that have the same total density λ_T.

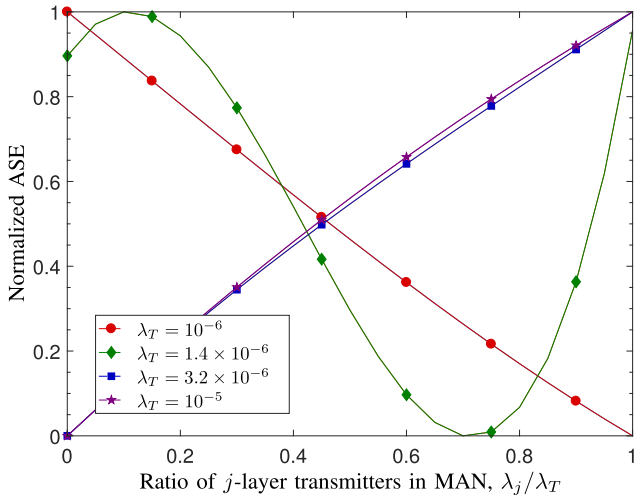

Fig. 12. Normalized ASE of two layer MAN according to the ratio of the j-layer transmitter density to the total density λ_j/λ_T with different total densities. λ_T when $h_j = 100$, $h_k = 200$, and $\tau =$ ts.

In order to further clarify the relationship between the total transmitter density λ_T and the optimal densities of each layer, we present the normalized ASE in Fig. 12 as a function of the ratio of the j-layer transmitter density to the total density λ_j/λ_T for different values of the total density λ_T. Here the normalized ASE, $\mathcal{S}_{\lambda_T}^{\mathcal{N}}(\rho)$, is defined as

$$\mathcal{S}_{\lambda_T}^{\mathcal{N}}(\rho) = (\mathcal{S}_{\lambda_T}(\rho) - \min_{\rho'} \mathcal{S}_{\lambda_T}(\rho'))/ \\ (\max_{\rho'} \mathcal{S}_{\lambda_T}(\rho') - \min_{\rho'} \mathcal{S}_{\lambda_T}(\rho')) \quad (41)$$

where $\mathcal{S}_{\lambda_T}(\rho)$ is the ASE for given total transmitter density λ_T and the ratio of j-layer transmitter density, $\rho = \lambda_j/\lambda_T$. Here, the normalized ASE is a linear transform that makes the ASE to have values between $[0, 1]$, for the optimal ratio visualization. From Fig. 12, we can see that when the total transmitter density λ_T is high, the optimal is to use the lower AN only, i.e., $\lambda_j^* = \lambda_T$. On the other hand, when λ_T is low, the optimal is to use the higher AN only, i.e., $\lambda_k^* = \lambda_T$. However, when λ_T is neither high nor low such as $\lambda_T = 1.4 \times 10^{-6}$, it is better to use the two layer MAN instead of the single layer AN, which is the same as the STP of the MAN with the receiver-oriented association.

VI. Conclusion

This paper establishes a foundation for the MAN accounting for the different UAV densities, altitudes, and transmission power in each layer AN. After modeling the MAN with the association rules and the channel, suitable for various scenario of the MAN, we newly analyze the association probability, the main link distance distribution, and the Laplace transform of the interference. We then analyze the STP and the ASE of the MAN, and also provide the upper bounds of the optimal UAV densities that maximize the STP and the ASE, which is decreasing with the altitude of the AN and determined independently without the effect of other layer UAV densities.

Finally, we provide some insights on the design of the MAN as follows: 1) the optimal density of AN, maximizing the ASE, decreases with the altitude of the layer; 2) the optimal UAV density of AN, maximizing the STP, decreases with the altitude of the AN for the receiver-oriented association case, while it becomes zero for the transmitter-oriented association case; and 3) the optimal design of MAN depend on the total density of MAN, where the optimal density ratio of AN with low altitude increases with the total density. Those outcomes can be usefully used as guidelines in the MAN design. Furthermore, this work can be a general framework, which can be used to develop techniques for enhancing the performance of the MAN, such as interference control, power control, and multi-input multi-output (MIMO) communications.

Appendix

A. Proof of Corollary 2

In this proof, we get the derivatives of the performance, then obtain the range of densities that reduce the performance. We use the following notation, that is not used in rest of the paper.

$$\mathcal{C}_{ij,\tau}^{(c)}(y) = \mathcal{A}_{ij,\tau}^{(c)} p_{ij,\tau}^{(c)}(y) f_{Y_{ij,\tau}^{(c)}}(y) \tag{42}$$

1) Receiver-Oriented Association: From Lemma 1, when $o = \mathrm{r}$, the derivative of the k-layer STP with respect to the j-layer transmitter density is given by

$$\frac{\partial}{\partial \lambda_{j,\mathrm{Tx}}} \mathcal{P}_{k,\tau} = \sum_{i \in \mathcal{K}, c \in \{\mathrm{L},\mathrm{N}\}} \frac{\partial \mathcal{C}_{ki,\tau}^{(c)}(y)}{\partial \lambda_{j,\mathrm{Tx}}} dy, \tag{43}$$

$$\frac{\partial \mathcal{C}_{ki,\tau}^{(c)}(y)}{\partial \lambda_{j,\mathrm{Tx}}} = \begin{cases} \dfrac{\mathcal{C}_{ki,\tau}^{(c)}(y)}{\lambda_{j,\mathrm{Tx}}} \left(1 - \lambda_{j,\mathrm{Tx}} \phi_{kj,\tau}^{(c)}(i,y)\right) & \text{for } i = j, \\ -\dfrac{\mathcal{C}_{ki,\tau}^{(c)}(y)}{\lambda_{j,\mathrm{Tx}}} \phi_{kj,\tau}^{(c)}(i,y) & \text{for } i \neq j, \end{cases} \tag{44}$$

$$\phi_{kj,\tau}^{(c)}(i,y) = 2\pi \sum_{c_\mathrm{o} \in \{\mathrm{L},\mathrm{N}\}} \left[\int_{h_{ki}}^{\infty} x \rho_{ki}^{(c_\mathrm{o})}(x) dx - \int_{\max\left(\chi_{kj,i,\tau}^{(c,c_\mathrm{o})}(x),\, h_{ki}\right)}^{\infty} \frac{x \rho_{ki}^{(c_\mathrm{o})}(x)}{1 + l_{ki}^{(c)}(y) P_i x^{-\alpha_{ki}^{(c_\mathrm{o})}}} dx \right] \tag{45}$$

When $i \neq j$, (44) is always negative. When $i = j$, if (46) holds, (44) is negative.

$$\max_{y,c} \left[1/\phi_{kj,\tau}^{(c)}(j,y) \right] \leq \lambda_{j,\mathrm{Tx}} \tag{46}$$

Here, $\phi_{kj,\tau}^{(c)}(j,y)$ increases with y and $\phi_{kj,\tau}^{(\mathrm{L})}(j,y) < \phi_{kj,\tau}^{(\mathrm{N})}(j,y)$, therefore, $\phi_{kj,\tau}^{(c)}(j,y)$ has minimum at the $c = (\mathrm{L})$ and $y = h_{kj}$, of which minimum is given by $\epsilon_{kj} = \phi_{kj,\tau}^{(\mathrm{L})}(j, h_{kj})$. Therefore, when $1/\epsilon_{kj} \leq \lambda_{j,\mathrm{Tx}}$, the STP of the k-layer is always decreased with the density of the transmitters in the j-layer, which gives the upper bound of the optimal density that maximizes the STP. In addition, the derivative of the ASE is given by

$$\frac{\partial}{\partial \lambda_{j,\mathrm{Tx}}} \mathcal{S}_{k,\tau} = \lambda_{k,\mathrm{Rx}} \sum_{i \in \mathcal{K}, c \in \{\mathrm{L},\mathrm{N}\}} R_{ki} \frac{\partial \mathcal{C}_{ki,\tau}^{(c)}(y)}{\partial \lambda_{j,\mathrm{Tx}}}. \tag{47}$$

The density of the receivers and the data rate are independent with the density of the transmitters. Therefore, if the inequality (46) holds, the ASE decreases with the density of the transmitters, which gives the same upper bound of the density that maximizes the STP.

2) Transmitter-Oriented Association: When $o = \mathrm{t}$, the derivative of the STP of the k-layer with respect to the density of the j-layer transmitter is given by

$$\begin{aligned} \frac{\partial}{\partial \lambda_{j,\mathrm{Tx}}} \mathcal{P}_{k,\tau} &= \sum_{i \in \mathcal{K}, c \in \{\mathrm{L},\mathrm{N}\}} \int_{h_{ik}}^{\infty} \frac{\partial \mathcal{C}_{ik,\tau}^{(c)}(y)}{\partial \lambda_{j,\mathrm{Tx}}}, \\ \frac{\partial \mathcal{C}_{ik,\tau}^{(c)}(y)}{\partial \lambda_{j,\mathrm{Tx}}} &= -\mathcal{C}_{ik,\tau}^{(c)}(y) \theta_{kj,\tau}^{(c)}(i,y) \qquad (48) \\ \theta_{kj,\tau}^{(c)}(i,y) &= 2\pi \sum_{c_\mathrm{o} \in \{\mathrm{L},\mathrm{N}\}} \int_{\max(\chi_{ik,j,\tau}^{(c,c_\mathrm{o})}, h_{ij})}^{\infty} x \rho_{ij}^{(c_\mathrm{o})}(x) \\ &\quad \times \left(1 - 1/\left(1 + l_{ij}^{(c)}(y) P_j x^{-\alpha_{ij}^{(c_\mathrm{o})}}\right)\right) dx, \qquad (49) \end{aligned}$$

Therefore, the STP always decreases with the transmitter density, which gives the optimal density as zero. In addition, the derivative of the ASE is given by

$$\frac{d}{d\lambda_{j,\mathrm{Tx}}} \mathcal{S}_{k,\tau} = \sum_{i \in \mathcal{K}, c \in \{\mathrm{L},\mathrm{N}\}} \int_{h_{ik}}^{\infty} R_{ik} \frac{\partial}{\partial \lambda_{j,\mathrm{Tx}}} \left(\lambda_{k,\mathrm{Tx}} \mathcal{C}_{ik,\tau}^{(c)}(y)\right), \tag{50}$$

$$\frac{\partial\left(\lambda_{k,\mathrm{Tx}}\mathcal{C}_{ik,\tau}^{(c)}(y)\right)}{\partial\lambda_{j,\mathrm{Tx}}} = \begin{cases} \mathcal{C}_{ik,\tau}^{(c)}(y)\left(1-\lambda_{j,\mathrm{Tx}}\theta_{kj,\tau}^{(c)}(i,y)\right) & \\ \qquad\qquad\qquad\qquad \text{for } k=j, \\ -\lambda_{k,\mathrm{Tx}}\mathcal{C}_{ik,\tau}^{(c)}(y)\theta_{kj,\tau}^{(c)}(i,y) \quad \text{for } k\neq j. \end{cases} \tag{51}$$

When $k \neq j$, the gradient is always negative which gives the optimal density as zero. When $k = j$, the range of the density that gives negative gradient is given by $\max_{i,y,c}\left[\frac{1}{\theta_{kj,\tau}^{(c)}(i,y)}\right] \leq \lambda_{j,\mathrm{Tx}}$. Note that we maximize over $i \in \mathcal{K}$. Here, as $\theta_{kj,\tau}^{(c)}(i,y)$ increases with y and $\theta_{kj,\tau}^{(\mathrm{N})}(i,y) < \theta_{kj,\tau}^{(\mathrm{L})}(i,y)$, the minimum is given as $\epsilon_{ik} = \theta_{kj,\tau}^{(\mathrm{L})}(i,h_{ki})$. Therefore, we get the upper bound of the transmitter density that maximizes the STP and the ASE.

B. Proof of Corollary 3

From Corollary 2, ϵ_{ij} is given by

$$\epsilon_{ij} = \int_0^\infty y\left(1-q(y,h_{ij})\right)dy,$$
$$q(y,h_{ij}) = \frac{\varrho_{ij}^{(\mathrm{L})}(y)}{1+\frac{\beta_{ij}h_{ij}^{\alpha_{ij}^{(\mathrm{L})}}}{(y^2+h_{ij}^2)^{\alpha_{ij}^{(\mathrm{L})}/2}}} + \frac{\varrho_{ij}^{(\mathrm{N})}(y)}{1+\frac{\beta_{ij}h_{ij}^{\alpha_{ij}^{(\mathrm{L})}}}{(y^2+h_{ij}^2)^{\alpha_{ij}^{(\mathrm{N})}/2}}}. \tag{52}$$

We use the integration by substitution for ϵ_{ij} as $y^2 = x^2 - h_{ij}^2$, hence, the modified LoS probability is $\varrho_{ij}^{(\mathrm{L})}(y) = \rho_{ij}^{(\mathrm{L})}\left(\sqrt{y^2+h_{ij}^2}\right)$ which increase with h_{ij} for given y. Therefore, ϵ_{ij} increases with h_{ij} if $q(y,h_{ij})$ decreases with h_{ij} for all $y \in [0,\infty)$. The function $q(y,h_{ij})$ is reformulated as

$$q(y,h_{ij}) = \frac{1}{1+\beta_{ij}\left(\frac{h_{ij}^2}{h_{ij}^2+y^2}\right)^{\alpha_{ij}^{(\mathrm{L})}/2}} + \frac{\varrho_{ij}^{(\mathrm{N})}(y)\beta_{ij}h_{ij}^{\alpha_{ij}^{(\mathrm{L})}}\left(\left(h_{ij}^2+y^2\right)^{\alpha_{ij}^{(\mathrm{N})}/2} - \left(h_{ij}^2+y^2\right)^{\alpha_{ij}^{(\mathrm{L})}/2}\right)}{\left(\beta_{ij}h_{ij}^{\alpha_{ij}^{(\mathrm{L})}}+\left(h_{ij}^2+y^2\right)^{\alpha_{ij}^{(\mathrm{N})}/2}\right)\left(\beta_{ij}h_{ij}^{\alpha_{ij}^{(\mathrm{L})}}+\left(h_{ij}^2+y^2\right)^{\alpha_{ij}^{(\mathrm{L})}/2}\right)}$$

We use $\varrho_{ij}^{(\mathrm{L})}(y) + \varrho_{ij}^{(\mathrm{N})}(y) = 1$. The upper part decreases with h_{ij} since $\frac{h_{ij}^2}{h_{ij}^2+y^2}$ increases with h_{ij}. Furthermore, the lower part decreases with h_{ij} if $1 < h_{ij}^2 + y^2$ and $1 < \beta_{ij}h_{ij}^{\alpha_{ij}^{(\mathrm{L})}}$. Therefore, ϵ_{ij} decreases with h_{ij} if $1 < h_{ij}$ and $1 < \beta_{ij}h_{ij}^{\alpha_{ij}^{(\mathrm{L})}}$.

REFERENCES

[1] D. Kim, J. Lee, and T. Q. S. Quek, "Performance analysis for multi-layer unmanned aerial vehicle networks," in *Proc. IEEE Globecom Workshops (GC Wkshps)*, Abu Dhabi, UAE, Dec. 2018, pp. 1–6.

[2] Y. Zeng, R. Zhang, and T. J. Lim, "Wireless communications with unmanned aerial vehicles: Opportunities and challenges," *IEEE Commun. Mag.*, vol. 54, no. 5, pp. 36–42, May 2016.

[3] N. H. Motlagh, M. Bagaa, and T. Taleb, "UAV-based IoT platform: A crowd surveillance use case," *IEEE Commun. Mag.*, vol. 55, no. 2, pp. 128–134, Feb. 2017.

[4] Y. Zeng *et al.*, "Throughput maximization for UAV-enabled mobile relaying systems," *IEEE Trans. Commun.*, vol. 64, no. 12, pp. 4983–4996, Dec. 2016.

[5] A. Al-Hourani, S. Kandeepan, and S. Lardner, "Optimal LAP altitude for maximum coverage," *IEEE Wireless Commun. Lett.*, vol. 3, no. 6, pp. 569–572, Dec. 2014.

[6] A. Al-Hourani, S. Kandeepan, and A. Jamalipour, "Modeling air-to-ground path loss for low altitude platforms in urban environments," in *Proc. IEEE Global Commun. Conf. (GLOBECOM)*, Austin, TX, USA, Dec. 2014, pp. 2898–2904.

[7] Z. Yang, L. Zhou, G. Zhao, and S. Zhou, "Blockage modeling for inter-layer UAVs communications in urban environments," in *Proc. Int. Conf. Telecommun*, Jun. 2018, pp. 307–311.

[8] M. Mozaffari, W. Saad, M. Bennis, and M. Debbah, "Unmanned aerial vehicle with underlaid device-to-device communications: Performance and tradeoffs," *IEEE Trans. Wireless Commun.*, vol. 15, no. 6, pp. 3949–3963, Jun. 2016.

[9] C. Liu, T. Q. S. Quek, and J. Lee, "Secure UAV communication in the presence of active eavesdropper," in *Proc. 9th Int. Conf. Wireless Commun. Signal Process.*, Nanjing, China, Oct. 2017, pp. 1–6.

[10] M. Kim and J. Lee, "Impact of an interfering node on unmanned aerial vehicle communications," *IEEE Trans. Veh. Technol.*, to be published.

[11] M. M. Azari, Y. Murillo, O. Amin, F. Rosas, M.-S. Alouini, and S. Pollin, "Coverage maximization for a poisson field of drone cells," in *Proc. IEEE PIMRC*, Oct. 2017, pp. 1–6.

[12] M. Alzenad and H. Yanikomeroglu, "Coverage and rate analysis for unmanned aerial vehicle base stations with LoS/NLoS propagation," in *Proc. IEEE Globecom Workshops (GC Wkshps)*, Abu Dhabi, UAE, Dec. 2018, pp. 1–7.

[13] T. Hou, Y. Liu, Z. Song, X. Sun, and Y. Chen, "Multiple antenna aided NOMA in UAV networks: A stochastic geometry approach," *IEEE Trans. Commun.*, vol. 67, no. 2, pp. 1031–1044, Feb. 2019.

[14] M. M. Azari, F. Rosas, A. Chiumento, and S. Pollin, "Coexistence of terrestrial and aerial users in cellular networks," in *Proc. IEEE Globecom Workshops (GC Wkshps)*, Dec. 2017, pp. 1–6.

[15] R. Arshad, L. Lampe, H. ElSawy, and M. J. Hossain, "Integrating UAVs into existing wireless networks: A stochastic geometry approach," in *Proc. IEEE Globecom Workshops (GC Wkshps)*, Dec. 2018, pp. 1–6.

[16] M. M. Azari, F. Rosas, and S. Pollin, "Cellular connectivity for UAVs: Network modeling, performance analysis, and design guidelines," *IEEE Trans. Wireless Commun.*, vol. 18, no. 7, pp. 3366–3381, Apr. 2019.

[17] C. Zhang and W. Zhang, "Spectrum sharing in drone small cells," in *Proc. IEEE Global Commun. Conf. (GLOBECOM)*, Washington, DC, USA, Dec. 2016, pp. 1–6.

[18] L. Qi, S. Yan, and M. Peng, "Modeling and performance analysis in UAV assisted ultra dense networks," in *Proc. IEEE Int. Conf. Commun. Conf.*, May 2018, pp. 1–6.

[19] H. Wu, X. Tao, N. Zhang, and X. Shen, "Cooperative UAV cluster-assisted terrestrial cellular networks for ubiquitous coverage," *IEEE J. Sel. Areas Commun.*, vol. 36, no. 9, pp. 2045–2058, Sep. 2018.

[20] X. Wang, H. Zhang, Y. Tian, and V. C. M. Leung, "Modeling and analysis of aerial base station-assisted cellular networks in finite areas under LoS and NLoS propagation," *IEEE Trans. Wireless Commun.*, vol. 17, no. 10, pp. 6985–7000, Oct. 2018.

[21] A. M. Hayajneh, S. A. R. Zaidi, D. C. McLernon, M. Di Renzo, and M. Ghogho, "Performance analysis of UAV enabled disaster recovery networks: A stochastic geometric framework based on cluster processes," *IEEE Access*, vol. 6, pp. 26215–26230, 2018.

[22] E. Turgut and M. C. Gursoy, "Downlink analysis in unmanned aerial vehicle (UAV) assisted cellular networks with clustered users," *IEEE Access*, vol. 6, pp. 36313–36324, 2018.

[23] V. V. Chetlur and H. S. Dhillon, "Downlink coverage analysis for a finite 3-D wireless network of unmanned aerial vehicles," *IEEE Trans. Commun.*, vol. 65, no. 10, pp. 4543–4558, Jul. 2017.

[24] J. Li and Y. Han, "Optimal resource allocation for packet delay minimization in multi-layer UAV networks," *IEEE Commun. Lett.*, vol. 21, no. 3, pp. 580–583, Mar. 2017.

[25] S. Sekander, H. Tabassum, and E. Hossain, "Multi-tier drone architecture for 5G/B5G cellular networks: Challenges, trends, and prospects," *IEEE Commun. Mag.*, vol. 56, no. 3, pp. 96–103, Mar. 2018.

[26] M. Haenggi and R. K. Ganti, "Interference in large wireless networks," *Found. Trends Netw.*, vol. 3, no. 2, pp. 127–248, 2009.

[27] Q. Wu and R. Zhang, "Common throughput maximization in UAV-enabled OFDMA systems with delay consideration," *IEEE Trans. Wireless Commun.*, vol. 66, no. 12, pp. 6614–6627, Dec. 2018.

[28] M. Alzenad, A. El-Keyi, F. Lagum, and H. Yanikomeroglu, "3-D Placement of an unmanned aerial vehicle base station (UAV-BS) for energy-efficient maximal coverage," *IEEE Wireless Commun. Lett.*, vol. 6, no. 4, pp. 434–437, Aug. 2017.
[29] S. Yan, M. Peng, and X. Cao, "A game theory approach for joint access selection and resource allocation in UAV assisted IoT communication networks," *IEEE Internet Things J.*, vol. 6, no. 2, pp. 1663–1674, Apr. 2019.
[30] C. Stöcker, R. Bennett, F. Nex, M. Gerke, and J. Zevenbergen, "Review of the current state of UAV regulations," *Remote Sens.*, vol. 9, no. 5, p. 459, 2017.
[31] S. Chandrasekharan *et al.*, "Designing and implementing future aerial communication networks," *IEEE Commun. Mag.*, vol. 54, no. 5, pp. 26–34, May 2016.
[32] H. S. Dhillon, R. K. Ganti, F. Baccelli, and J. G. Andrews, "Modeling and analysis of K-tier downlink heterogeneous cellular networks," *IEEE J. Sel. Areas Commun.*, vol. 30, no. 3, pp. 550–560, Apr. 2012.
[33] S. Singh, H. S. Dhillon, and J. G. Andrews, "Offloading in heterogeneous networks: Modeling, analysis, and design insights," *IEEE Trans. Wireless Commun.*, vol. 12, no. 5, pp. 2484–2497, May 2013.
[34] Q. Zhang, H. H. Yang, T. Q. S. Quek, and J. Lee, "Heterogeneous cellular networks with LoS and NLoS transmissions—The role of massive MIMO and small cells," *IEEE Trans. Wireless Commun.*, vol. 16, no. 12, pp. 7996–8010, Dec. 2017.
[35] H. Cho, C. Liu, J. Lee, T. Noh, and T. Q. S. Quek, "Impact of elevated base stations on the ultra-dense networks," *IEEE Commun. Lett.*, vol. 22, no. 6, pp. 1268–1271, Jun. 2018.
[36] B. Galkin, J. Kibiłda, and L. A. DaSilva, "A stochastic geometry model of backhaul and user coverage in urban UAV networks," Oct. 2017, *arXiv:1710.03701*. [Online]. Available: https://arxiv.org/abs/1710.03701
[37] R. Amorim, H. Nguyen, P. Mogensen, I. Z. Kovács, J. Wigard, and T. B. Sørensen, "Radio channel modeling for UAV communication over cellular networks," *IEEE Wireless Commun. Lett.*, vol. 6, no. 4, pp. 514–517, Aug. 2017.
[38] *Propagation Data and Prediction Methods Required for the Design of Earth-Space Telecommunication Systems*, document Rec. ITU-R P.618-13, 2015.
[39] T. Bai, R. Vaze, and R. W. Heath, Jr., "Analysis of blockage effects on urban cellular networks," *IEEE Trans. Wireless Commun.*, vol. 13, no. 9, pp. 5070–5083, Sep. 2014.
[40] M.-S. Alouini and A. J. Goldsmith, "A unified approach for calculating error rates of linearly modulated signals over generalized fading channels," *IEEE Trans. Commun.*, vol. 47, no. 9, pp. 1324–1334, Sep. 1999.
[41] V. Chandrasekhar and J. G. Andrews, "Spectrum allocation in tiered cellular networks," *IEEE Trans. Commun.*, vol. 57, no. 10, pp. 3059–3068, Oct. 2009.

Dongsun Kim (S'18) received the B.E. degree from the School of Undergraduate Studies, Daegu Gyeongbuk Institute of Science and Technology (DGIST), Daegu, South Korea, in 2018, where he is currently pursuing the Ph.D. degree with the Department of Information and Communication Engineering. His research interests include machine learning-based network intelligence and ultra-dense network design.

Jemin Lee (S'06–M'11) received the B.S. (Hons.), M.S., and Ph.D. degrees in electrical and electronics engineering from Yonsei University, Seoul, South Korea, in 2004, 2007, and 2010, respectively. She was a Post-Doctoral Fellow with the Massachusetts Institute of Technology (MIT), Cambridge, MA, USA, from 2010 to 2013, and a Temasek Research Fellow with the iTrust, Centre for Research in Cyber Security, Singapore University of Technology and Design (SUTD), Singapore, from 2014 to 2016. She is currently an Associate Professor with the Department of Information and Communication Engineering, Daegu Gyeongbuk Institute of Science and Technology (DGIST), Daegu, South Korea. Her current research interests include wireless communications, wireless security, intelligent networking, and machine-type communications.

Dr. Lee received the IEEE ComSoc AP Outstanding Paper Award in 2017, the IEEE ComSoc AP Outstanding Young Researcher Award in 2014, the Temasek Research Fellowship in 2013, the Chun-Gang Outstanding Research Award in 2011, and the IEEE WCSP Best Paper Award in 2014. She serves as a Vice-Chair for the IEEE ComSoc Radio Communications Technical Committee (RCC) and a Secretary for the IEEE ComSoc Asia-Pacific Board. She was an Editor for the IEEE COMMUNICATIONS LETTERS from 2014 to 2019. She is currently an Editor for the IEEE TRANSACTIONS ON WIRELESS COMMUNICATIONS.

Tony Q. S. Quek (S'98–M'08–SM'12–F'18) received the B.E. and M.E. degrees in electrical and electronics engineering from the Tokyo Institute of Technology, Tokyo, Japan, in 1998 and 2000, respectively, and the Ph.D. degree in electrical engineering and computer science from the Massachusetts Institute of Technology, Cambridge, MA, USA, in 2008. He is currently the Cheng Tsang Man Chair Professor with the Singapore University of Technology and Design (SUTD). He is also the Acting Head of ISTD Pillar, a Sector Lead of the SUTD AI Program, and the Deputy Director of the SUTD-ZJU IDEA. His current research topics include wireless communications and networking, network intelligence, Internet-of-things, URLLC, and big data processing.

Dr. Quek has been actively involved in organizing and chairing sessions and has served as a member for the Technical Program Committee and as symposium chairs in a number of international conferences. He received the 2008 Philip Yeo Prize for Outstanding Achievement in Research, the 2012 IEEE William R. Bennett Prize, the 2015 SUTD Outstanding Education Awards—Excellence in Research, the 2016 IEEE Signal Processing Society Young Author Best Paper Award, the 2017 CTTC Early Achievement Award, the 2017 IEEE ComSoc AP Outstanding Paper Award, and the 2016–2018 Clarivate Analytics Highly Cited Researcher. He was an Executive Editorial Committee Member for the IEEE TRANSACTIONS ON WIRELESS COMMUNICATIONS, an Editor for the IEEE TRANSACTIONS ON COMMUNICATIONS, and an Editor for the IEEE WIRELESS COMMUNICATIONS LETTERS. He is currently serving as an Editor for the IEEE TRANSACTIONS ON WIRELESS COMMUNICATIONS, the Chair of the IEEE VTS Technical Committee on Deep Learning for Wireless Communications, and an Elected Member of the IEEE Signal Processing Society SPCOM Technical Committee. He is a Distinguished Lecturer of the IEEE Communications Society.